Master Erasmus Mundus in Photonics Engineering, Nanophotonics and Biophotonics

Europhotonics

MASTER THESIS WORK

CHARACTERIZATION OF MOLECULAR ORIENTATION IN SUPER-RESOLUTION FLUORESCENCE MICROSCOPY

Yibing ZHAO

Supervised by Dr. Melike Lakadamyali, (ICFO)
And Prof. Uli Nienhaus, (KIT)

Presented in Barcelona, on 6th September 2012

Registered at

Escola Tècnica Superior d'Enginyeria de Telecomunicació de Barcelona

Characterization of molecular orientation in super-resolution fluorescence microscopy

This thesis has been carried out by ZHAO Yibing

at The Institute of Photonic Sciences (ICFO), 08860Castelldefels (Barcelona), Spain

under the supervision of

Professor Melike Lakadamyali (ICFO)

And Prof. Uli Nienhaus (KIT)

Abstract

Fluorescence microscopy is widely applied to study biological processes. However, the resolution of far-field fluorescence imaging was limited by diffraction. Recent developments of super-resolution fluorescence microscopy techniques, such as stochastic optical reconstruction microscopy (STORM) and photo-activated localization microscopy (PALM), overcome the diffraction limit and allow the observation of many biological structures not re-solvable in conventional fluorescence microscopy.

STORM and PALM strongly rely on precisely and accurately determining the position of individual molecules. A number of factors can affect the precision and accuracy in determining the position of single molecules. One of these factors is the orientation of the molecule's dipole moment, which is the subject of this thesis.

In this thesis we aim to characterize the effect of molecular dipole orientation on the resolution of super-resolution fluorescence microscopy techniques that rely on single molecule detection and localization.

Keywords: stochastic optical reconstruction microscopy (STORM), photoactivated localization microscopy (PALM), super-resolution fluorescence microscopy, molecular orientation

Acknowledgement

First and foremost, I would like to show my deepest gratitude to my supervisor, Prof. Melike Lakadamyali from The Institute of Photonics Sciences (ICFO), who provided me with valuable guidance and stimulating encouragement throughout all the time of research for and writing of this thesis. I shall also extend my thanks to my co-supervisor, Prof. Uli Nienhaus from The Karlsruhe Institute of Technology (KIT).

My group colleagues from Advanced Fluorescence Imaging and Biophysics group supported me in my research work. I want to thank them for all their help, support, interest and valuable hints. Especially I am obliged to Stefan Balint, NelaDurisic, Ángel Sandoval Álvarez, Ione Verdeny Vilanova, Anna Oddone, Johnny Tam and Lara Laparra. I also want to thank the former group member Norman Brede for all his assistance on computer programming and data analysis. My thesis depends to a great extent on his previous work.

Especially, I would like to give my special thanks to all my Erasmus Mundus Europhotonics friends, for the company of these two years study. Last but not least, I would like to thank to my family whose patient love enabled me to complete my master study.

Contents

Chapter 1 Introduction

1.1. Fluorescence microscopy in biology

Fluorescence microscopy has been playing an increasingly important role in biology, being one of the most widely used tools in biological and biomedical research in the past few decades.

The basic principle of a fluorescence microscope is to illuminate a specimen with a desired and specific band of wavelengths. The emission spectrum of fluorophore is shifted in comparison to the excitation spectrum, generally to a longer wavelength as a result of energy loss. Because of this phenomenon which is known as Stokes Shift, it becomes easy to separate the emission light from the brighter excitation light by simply using spectral filters [1].

However, not all the molecules or proteins possess natural fluorescence, which is called intrinsic fluorescence. Instead, an extrinsic fluorophore is typically used to tag a biological target with high specificity [1]. Due to its inherent non-invasiveness, fluorescence imaging enables to observe cellular components or real-time processes in living cells through molecule-specific labelling [2].

Furthermore, compared to transmitted or reflected light microscopy, fluorescence imaging involves the detection of a bright signal against a dark background, greatly improving image contrast [3].

1.2. Diffraction limit

Unfortunately, conventional fluorescence microscopy is limited by relatively low spatial resolution because light is a wave and is subject to diffraction [4]. A point source of light passing through a microscope generates a central spot with diffraction pattern,

called airy disc. The intensity profile of the blurred spot is defined as point spread function (PSF) (Figure 1) of the microscope. The full width at half maximum (FWHM) of the PSF in the lateral (x, y) and axial (z) directions was recognized by Abbe in the 19th century [5] and later refined by Lord Rayleigh in 1896, who introduced the Rayleigh criterion (the smallest distance two point sources can approach each other and still be resolvable):

$$\Delta x, \Delta y = \frac{\lambda}{2(\mathrm{n}\sin\theta)} \quad in\ lateral$$

$$\Delta z = \frac{2\lambda}{(n\sin\theta)^2} \quad in\ axial$$

where λ is the wavelength of light, n is the index of refraction of the medium, and θ is the half-cone angle of the optical objective lens. The denominator $n\,sin\,\theta$ is called the numerical aperture (NA).

This minimum size determines the achievable resolution, which can be considered as the smallest separation distance d between two point-like objects, as illustrated in Figure 2. When $d \gg \Delta x, \Delta y$, they can be well distinguished as individual emitters. Once they move close to each other, at $d \approx \Delta x, \Delta y$, the PSFs will overlap and they will be barely resolvable. If they move further closer, they will no longer be resolvable.

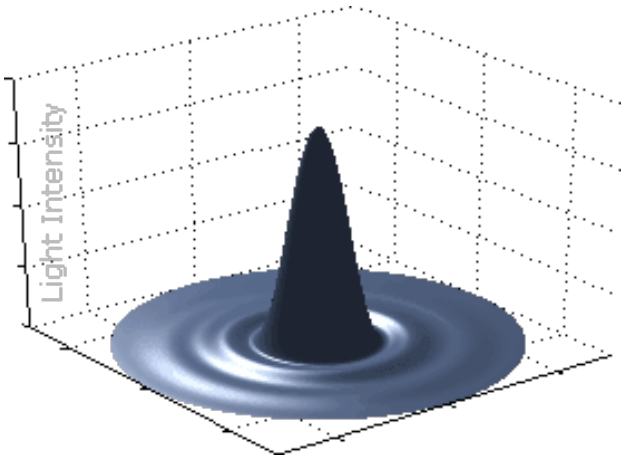

Figure 1 3-D visualization of point spread function (PSF).

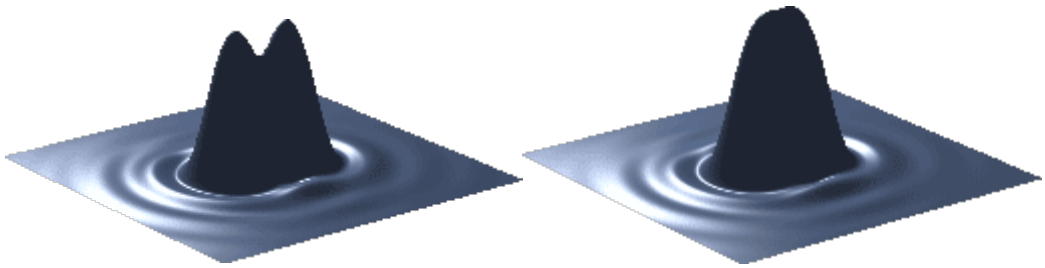

(a) (b)

Figure 2 (a) 3-D visualization of two barely resolved spots (b) 3-D visualization of two non-resolved spots

As a result, the highest achievable point-to-point resolution which can be obtained with an optical microscope is governed by the characteristics of its objective and inversely proportional to the wavelength of imaging light. This limit cannot be easily overcome by rational alternations in objective lens or aperture design.

Nowadays, numerical aperture could reach about 1.4 with oil immersion objectives. In practice, when imaging with visible light ($\lambda \approx 550nm$), the resolution is around 200 nm laterally. For conventional fluorescence microscopy, it is classically about 200–300 nm in the lateral direction and 500–700 nm in the axial direction. This is larger than the molecular structures, and comparable to many subcellular structures which span a range of length scales from micrometres to nanometres. Therefore the optical resolution of a conventional microscope leaves a large gap that cannot be explored and has a tremendous impact on our understanding of biology in detail [2].

Near-field microscopy [6] is one of the earliest techniques developed that could achieve high spatial resolution by exploiting the properties of evanescent waves. However it is expensive, limited to studying only the sample surfaces and not applicable to *in vivo* samples.

There are several far-field imaging methods that push the diffraction barrier to smaller values [4], like 4Pi microscopy [7], I5M (the combination of illumination interference microscopy (I2M) and incoherent imaging interference microscopy (I3M)) [8] and

structured-illumination microscopy (SIM) [9]. Although they improve the axial resolution to ~250 nm (in 4Pi and I5M) and the lateral resolution to ~100 nm (in SIM), these techniques fall short of truely breaking the diffraction barrier.

1.3. Super-resolution fluorescence microscopy

In recent years, a number of groups have successfully invented new techniques to achieve spatial resolution beyond the diffraction limit described above. This new field is called super-resolution microscopy. These methods have yielded one order of magnitude improvement in spatial resolution in all three dimensions over conventional fluorescence microscopy [4] and broaden the range of possible applications of fluorescence microscopy in the biomedical sciences.

The super-resolution microscopy can be categorized into two main types, spatially patterned excitation based techniques and single molecule localization based techniques.

1.3.1. Spatially patterned excitation based techniques

Among the spatially patterned excitation based techniques, the concept of stimulated emission depletion (STED) microscopy was the first to break the diffraction barrier. It was proposed by Stefan Hell in 1994 [10] and the first experimental demonstration was achieved in 1999 [11]. It takes advantage of non-linear de-excitation of fluorescent dyes to overcome Abbe's diffraction limit.

Two concentric laser beams are used in STED microscopy. The first beam, an excitation laser with wavelength of λ_{exc}, pumps fluorophores from their ground stateS_0 their excited state S_1, see Figure 3. Spontaneous fluorescence emission brings the fluorophore back to the ground state S_0. However, before spontaneous emission can happen, another laser, the STED beam with red-shifted wavelength ($\lambda_{STED} > \lambda_{exc}$), forces the excited fluorophores to transit from the excited state to the ground state via stimulated emission.

A phase mask is placed in the light path of the STED laser to modulate its phase-spatial distribution and to generate a donought-shaped pattern in the *xy* plane.

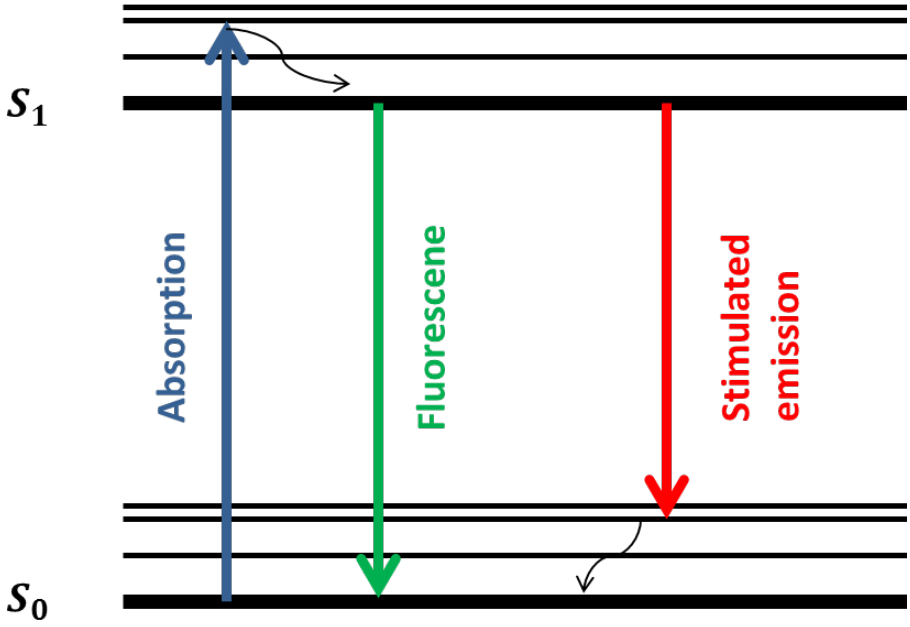

Figure 3 The principle of stimulated emission depletion (STED) microscopy.

This donought pattern has zero intensity at the centre of the excitation laser and non-zero intensity on the periphery. With saturated depletion, the fluorescence region near the centre point is suppressed, leading to a decreased size of the effective point spread function (PSF), demonstrated in Figure 4. Controlling the intensity and the profile of STED beam is the key that determines resolution.

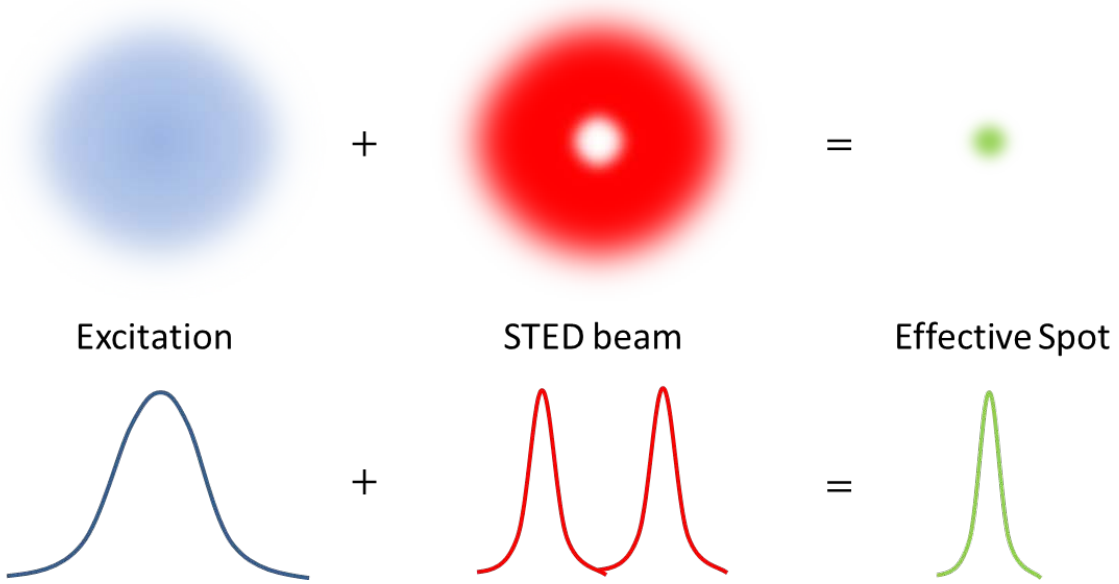

Figure 4 In STED, a donought shaped STED laser is applied with the zero point overlapped with the maximum of the excitation laser, leading a small size effective spot.

After almost one decade development, STED has provided spatial resolutions down to 20nm in lateral and 30-40 nm in the axial dimension [12] [13]. In cells, a remarkable resolution of $45 \times 45 \times 108$ nm has been achieved for 3D imaging [14].

1.3.2. Single molecule localization based techniques

The other variant of super-resolution microscopy is known as single molecule localization based techniques. These techniques rely on the concept that the position of a single molecule can be determined with nanometer precision [1]. However, in a densely labelled biological sample, fluorescence emission from many molecules overlap in a diffraction limited volume, making it challenging to determine the position of individual molecules. To overcome this problem, these techniques take advantage of a new generation of photo-activatible and photo-switchable fluorophores that have been discovered in the past few years [16] [17]. These fluorophores can switch between a fluorescent and dark state. It is then possible to use light excitation to switch on the fluorescence of only a small subset of these fluorophores at any one time. Therefore, spatial overlapping fluorescent images can be separated in the time domain. It is then

conceivable that super-resolution can be achieved by determining the position of each fluorescent probe in the sample with high precision and reconstructing an image from these positions. This concept has been independently conceived and implemented in several labs simultaneously and has been referred to as: stochastic optical reconstruction microscopy (STORM) [18], photo-activated localization microscopy (PALM) [19], and fluorescence photoactivation localization microscopy (FPALM) [20]. The details of these techniques will be introduced in Chapter 2.

1.4. Structure of this thesis

The goal of this thesis is to characterize the effect of molecular orientation on the resolution of super-resolution fluorescence microscopy techniques that rely on single molecule detection and localization.

Chapter 1 introduces the current state of development and future challenges of super-resolution microscopy techniques.

Chapter 2 reviews the principle of super-resolution fluorescence microscopy by single molecule imaging, as well as its localization precision and accuracy that can be achieved.

Chapter 3 presents the experimental methods used to characterize the effect of molecular orientation on the resolution of super-resolution fluorescence microscopy.

The results are given and discussed in Chapter 4 and Chapter 5 respectively.

Chapter 2 Super-resolution fluorescence microscopy by single molecule imaging

2.1. Localization precision in single fluorophore imaging

Although the image of a single isolated fluorphore appears as a diffraction-limited spot, its position can be determined much more precisely by finding the centroid of its image. The precise determination can be easily achieved by curve-fitting the point spread function (PSF) of the diffraction limited image to a Gaussian function. Thus, the localization precision is given approximately by

$$\Delta \approx \sqrt{\frac{s^2 + \frac{a^2}{12}}{N} + \frac{4\sqrt{\pi} s^3 b^2}{aN^2}}$$

where Δ is the localization precision, s is the standard deviation of the PSF, a is the pixel size, N is the number of photons detected from the fluorophore and b is the standard deviation of the image background [15].

It can be reformed as below,

$$\Delta \approx \sqrt{\frac{s^2}{N} + \frac{\frac{a^2}{12}}{N} + \frac{4\sqrt{\pi} s^3 b^2}{aN^2}}$$

The first term of the equation is the photon noise, the second is due to the increase in error due to the edge size a of the pixels in the image, and the third term takes the background noise b into account [21].

Therefore, if the number of photons detected for each fluorophore is large enough, so as to clearly distinguish individual PSF from surrounding background, the fluorophore can be precisely located, despite the fact that its image is broad due to diffraction. Based on

this concept, Prof. Paul R. Selvin's group has shown that the localization of a single fluorescence molecule can be achieved with ~1.5 nm precision [22].

However, this cannot be directly translated into image resolution. The ability to resolve a single molecule in a diffraction limited region does not imply the ability to resolve arbitrarily complicated structures at the same scale. When multiple fluorophores are positioned close to each other with the separation distance less than PSF width, their images will overlap and individual fluorophores can no longer be distinguished and fit to a Gaussian to find their positions.

2.2. Principle of super-resolution fluorescence microscopy using single-molecule localization

A typical fluorescently labelled sample contains a high density of fluorophores with hundreds or thousands of fluorophores per diffraction-limited region, making them difficult to resolve. However, if we can temporally separate the single molecule from the adjacent cluster of molecules, in other words, if it is possible to image only a sparse subset of fluorophores in the field of view at one time, then their positions can be fit and determined with high precision.

This concept of single molecule localization microscopy has been independently conceived and implemented by different groups in 2006, stochastic optical reconstruction microscopy (STORM) by Prof. Xiaowei Zhuang [18], photo-activated localization microscopy (PALM) by Prof. Eric Betzig and co-inventor Prof. Harald Hess [23], and fluorescence photoactivation localization microscopy (FPALM) by Prof. Samuel T. Hess [20], respectively, yielding resolution down to 20~30 nm.

All these three methods use photo-activatible and photo-switchable fluorescent dyes or proteins. The diffraction-limited molecules can be activated at different times by an activation laser with a wavelength different from the imaging laser, so that the

molecules can be individually imaged and deactivated. Repeated cycles of activation, imaging and deactivation make it possible to map their positions and reconstruct a high resolution image.

In 2002, George H. Patterson and Prof. Jennifer Lippincott-Schwartz first reported a photoactivatable variant of GFP (PA-GFP) which is dark in its native state but increases fluorescence tremendously when excited by 488nm light after intense irradiation with 413nm light [24]. Prof. Eric Betzig has used this characteristic of PA-GFP to achieve the on-off states of the fluorophore in response to light in PALM.

While PALM and FPALM have taken advantage of genetically encoded fluorescent proteins, STORM on the other hand, exploits the photo-switching properties of synthetic fluorophores. Mark Bates and Prof. Xiaowei Zhuang have discovered that when some synthetic dyes are paired together (for example Cy3 and Cy5) they behave like an optical switch and the fluorescence of one of the dyes (the reporter) can be turned on and off by illuminating with laser light that matches the excitation spectrum of the second dye (activator) [3]. They have later used these and other dye pairs to achieve the photoswitching needed for super-resolution imaging in STORM [18] [25]. All the fluorophores are first constrained to the dark state by illuminating with a strong imaging laser, afterwards, only a few of them are excited per imaging cycle by the activation laser and the cycle is repeated many times. This procedure is shown in Figure 5. Therefore, like a PALM image, a STROM image is also a composite of all the single molecule positions.

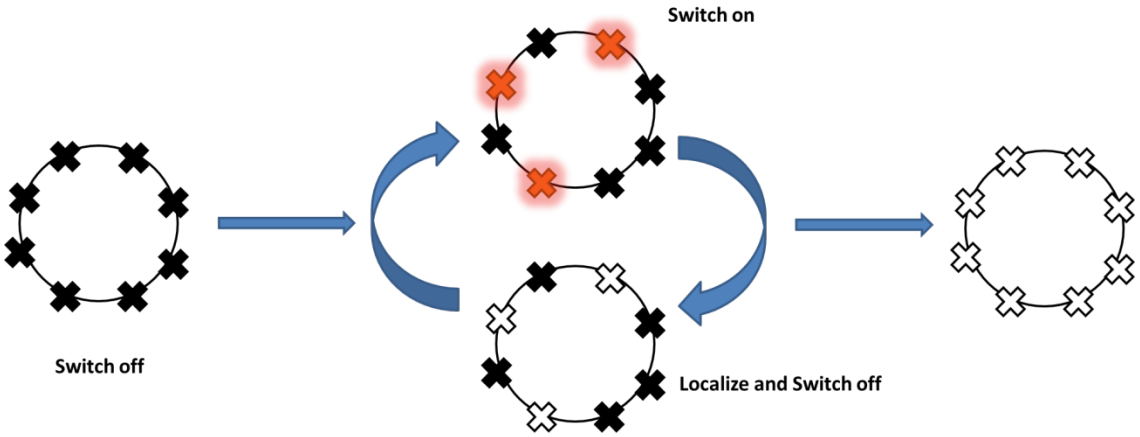

Figure 5 STORM imaging procedure.

Moreover, when the images of individual molecules are collected to generate a two-dimensional STORM image, they also contain information that reveals their positions in the third dimension. 3-D STROM imaging has been demonstrated by inserting a cylindrical lens into the imaging path of the microscope to introduce astigmatism to the PSF which encodes the z-position of the molecule [26].

The addition of the third dimension is one of a series of improvements to the original STORM technique. More compatible new fluorescent labels and faster data analysis [3] show the great promise of super-resolution fluorescence microscopy in the study of biological processes at the sub-cellular and molecular scale.

2.3. Localization precision and accuracy

The super-resolution microscopy has dramatically improved the spatial resolution over conventional fluorescence microscopy. We have already summarized the basic concept of precisely localizing single fluorophores. Since the actual molecular position is unknown in advance, its coordinate is determined by centroid calculation via the image that is projected onto the camera [27]. Clearly, the reliability of the images and the final

resolution, depends on both the precision and accuracy by which the positions can be determined [28].

In this section, we discuss factors that limit the localization precision and accuracy in super-resolution fluorescence microscopy and potential ways to overcome these limits.

Before we investigate all parameters at play, first we clear up the distinction between localization precision and accuracy.

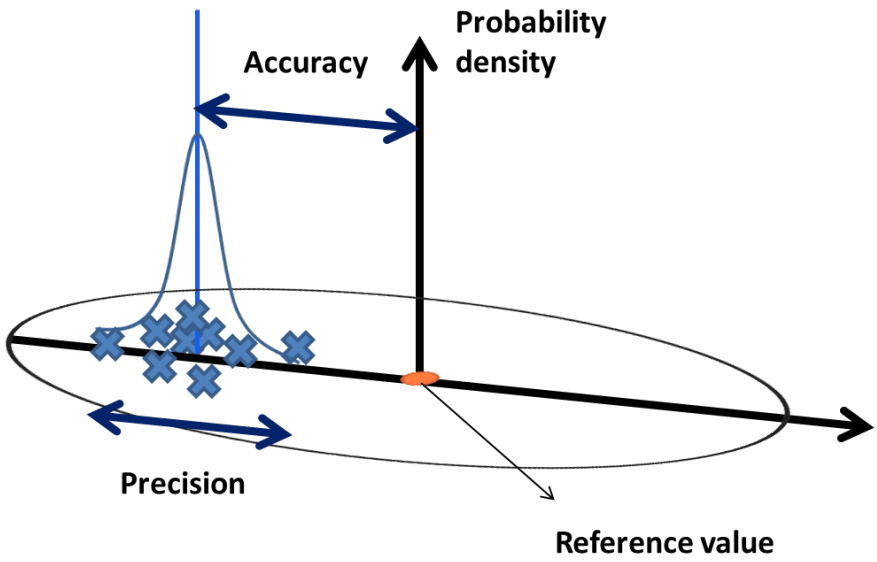

Figure 6 Precision and accuracy.

Accuracy estimates closeness between a measured quantity value and a true quantity value, while precision presents similarity of measured quantity values obtained which relate to statistical error [29]. In other words, precision stands for the reliability of the experiment, or how reproducible the experiment is. The accuracy is a measure of how closely the experimental results agree with a true value.

2.3.1. Localization precision

A number of factors need to be considered when attempting to localize individual molecules for super-resolution fluorescence microscopy by single molecule approach.

Among the critical elements that affect localization precision are photons collected from a fluorophore background signal, and stage drift, all of which can affect the resolution of the final image [4].

The localization precision can be determined by localizing the same molecule in many cycles. Since each time the molecule's position is determined, there will be some error in this determination. Therefore the positions will form a small cluster and the size of this cluster is a measure of how precisely a molecule can be localized. To compensate for stage drift, fluorescent beads are immobilized on glass. Drift can be determined and subtracted from molecule positions by tracking the position of these fluorescent beads.

2.3.2. Localization accuracy

While parameters such as drift, fluorophore brightness and background can be controlled in an experiment to a certain extend, one parameter that can affect resolution by affecting localization accuracy but cannot be easily controlled is the molecular dipole orientation. Notably, the dipole characteristics of molecules generally yield asymmetric fluorescence patterns PSF, see Figure 7. This asymmetry is negligible in conventional fluorescence microscopy. However, it can seriously limit the localization accuracy in the super-resolution methods employing single molecule localization [30].

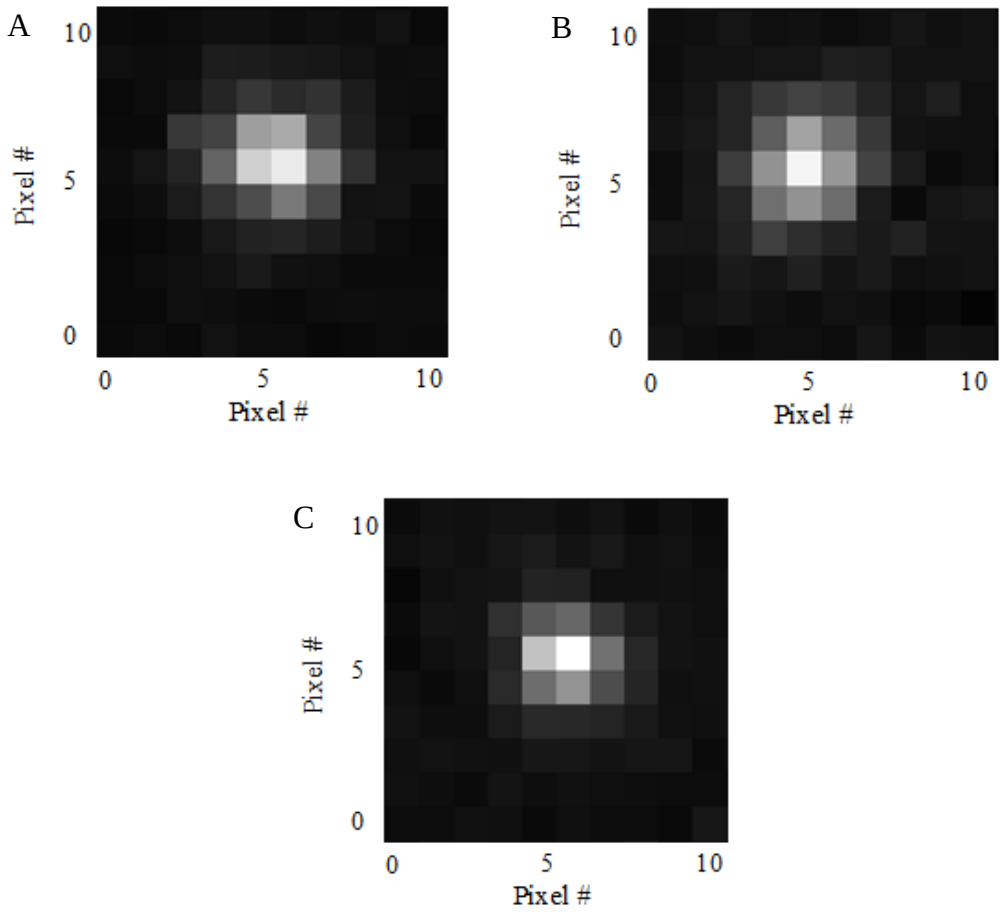

Figure 7 Point spread functions for different fixed molecules with different spatial orientations.

Engelhardt et. al. pointed out that the orientation of the dipole moment of single emitters plays a crucial role in localization accuracy in super-resolution fluorescence microscopy [30]. A systematic error comes into play when molecule dipole is titled at an angle with respect to the focal plane. While this tilt does not lead to any errors in localization when the molecule is in the focal plane, it can lead to large errors in localization if the molecule is a few hundred nanometers away from the focal plane. Figure 8 demonstrates that if the molecular dipole (in red arrow) is parallel to the focal plane (*x*,*y* plane), the position projected on the imaging plane is at the very same place irrespective of the molecule's position on the optical axis (*z*-axial). However, while the position of a molecule with a tilt angle β can be accurately determined when it is exactly in focus, a significant error will be introduced to the position determination if it

is slightly shifted from the focal plane along the optical axis. If the position of this molecule is measured at different focal planes, there will be a displacement in the position measured at one focal plane compared to the one measured at another focal plane. The amount of displacement will depend on the tilt angle β.

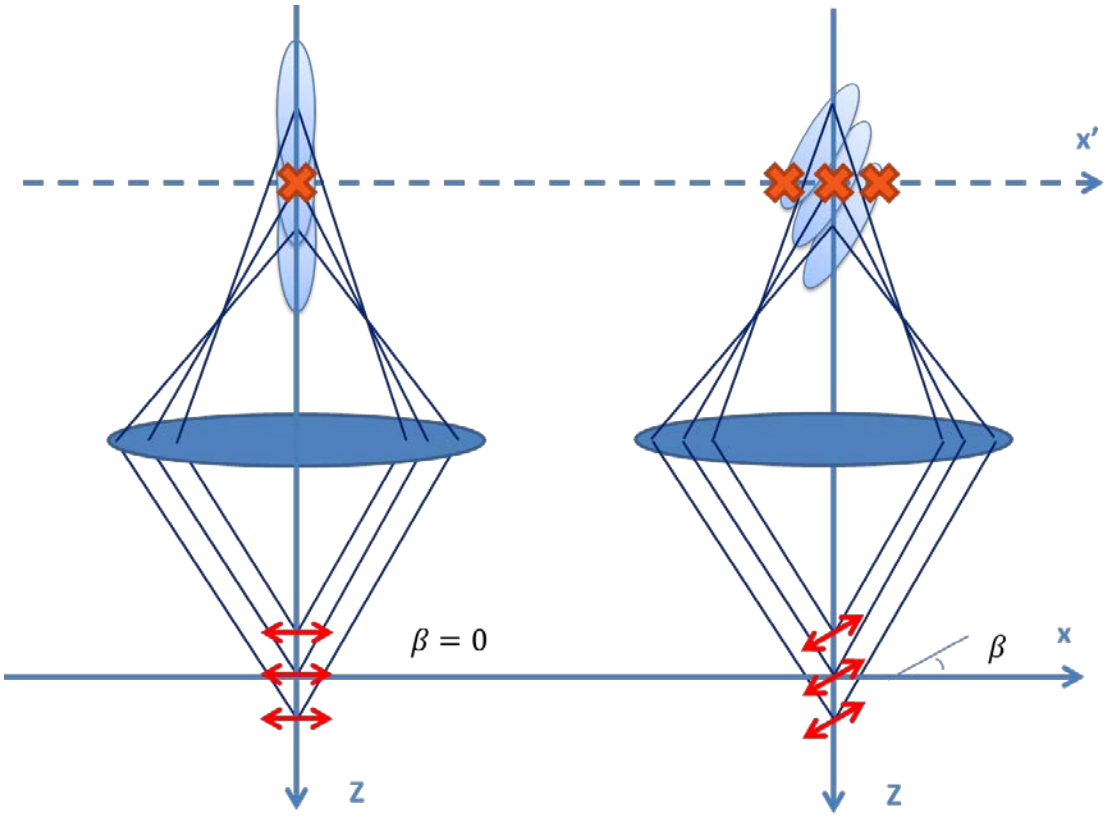

Figure 8. Displacement in a molecules position that results from molecular orientation. (A) When the molecule (red arrow) is not tilted with respect to the optical axis, x and y position of the observed spot (red cross) is not displaced, even when it is out of focus. (B) When the molecule is tilted, the PSF also becomes tilted with respect to the optical axis, causing a displacement in xy (Adapted from Engelhardt et. al. [30])

In practice, a typical molecule localized in the final super-resolution fluorescence microscopy image can be as far away as 200nm to 300nm from the focal plane. Therefore in principle the molecular dipole orientation of the molecule can lead to large errors in localization accuracy and degrade the resolution of the final image. The largest effect will be for molecules whose dipole orientation is fixed at a certain large tilt angle

with respect to the focal plane. However, such molecules will likely not be effectively excited by the imaging laser and their peak intensity will be lower than the molecules whose dipole is parallel to the focal plane. In Engelhardt et. al. experiment, a molecule at $z = 0$, when it is tilted out of the focal plane, for example, at $z \approx 33°$, the peak intensity is half of that of the untilted dipole [30]].

Therefore these molecules may be filtered out from the final image and not introduce as large an error as expected. In general the exact effect of the molecular orientation in the image resolution of super-resolution microscopy has not been fully characterized.

Engelhardt et. al. characterized the displacement obtained in the position of a fluorescent molecule which has been spin coated onto glass when it is in focus or +/-300 nm out of focus [30]. They find that large displacements in position can result from errors in localizing the position of those molecules whose molecular orientation is tilted. However, in a real STORM experiment, it is not the ordinary practice to spin coat molecules onto glass, which gives rise to a completely fixed molecular dipole orientation. Instead the fluorophores are attached by a flexible linker to an antibody and they are likely free to rotate, therefore possibly cancelling out any effects due to molecular orientation. The purpose of this thesis is to characterize the errors to localization accuracy in a realistic STORM experiment due to the molecular dipole orientation.

Chapter 3 Experimental methods

3.1. Optical setup

The microscope used in the experimentsis was built around an Olympus IX71 inverted frame. A schematic setup is shown in Figure 9. An Argon-Krypton laser running in the multi-wavelength mode provides a variety of wavelengths. These wavelengths are spectrally split with a prism and 457nm, 488nm, 514nm and 647nm lines are combined by using dichroic mirrors. These lines are further combined with illumination from two solid state lasers: 405nm and 560nm. In the experiments performed for this thesis, 560nm is the most frequently-used wavelength to excite Cy3. An acousto-optical tunable filter (AOTF) is used for adjusting the intensity of each wavelength and as a shutter. The AOTF is controlled by a custom-written LabView software.

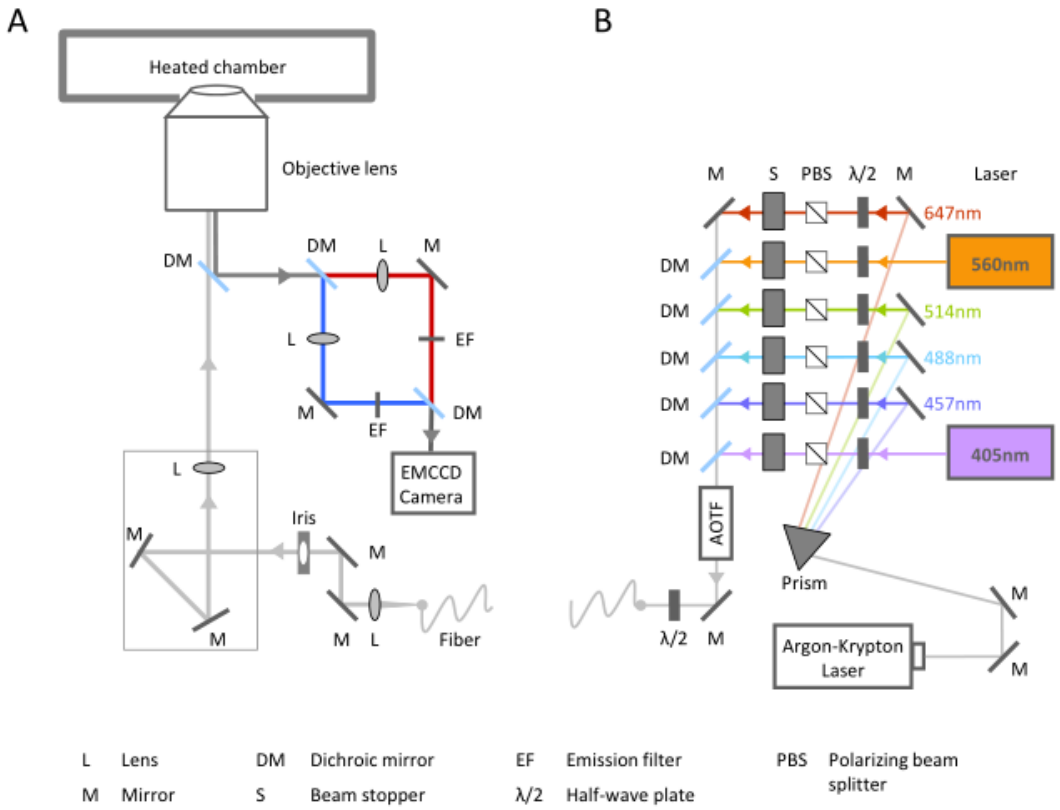

Figure 9 Microscope optical setup. (A) Schematic drawing of the illuminating and imaging path of our custom built microscope. (B) Light sources. (Figure adapted from Norman Brede [31])

The lasers and microscope frame are placed on separate optical tables to isolate the microscope from laser vibrations. The sample is imaged using a total internal reflection fluorescence (TIRF) microscope equipped with an oil immersion objective with a numerical aperture (NA) of 1.4. The incoming collimated laser beam can be shifted such that it enters the objective close to the edge of the objective rather than at the center. This allows the beam to reach the glass/water interface at an angle larger than the critical angle, leading to total internal reflection. At the interface an exponentially decaying evanescent field is generated and excites the sample, see Figure 10.

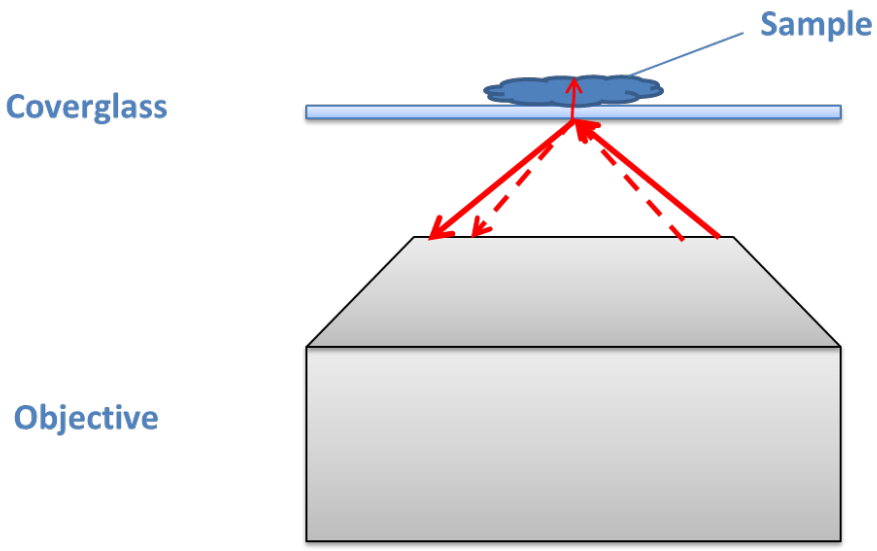

Figure 10 Total internal reflection fluorescence (TIRF) microscope. The red dotted lines are the light path of critical angle of total internal reflection. In order to satisfy the total internal reflection condition, the incoming collimated laser beam (red line) has an angle larger than the critical angle when it reaches the glass/water interface. At the interface an exponentially decaying evanescent field is generated and excites the sample.

Motorized xy-stage is used to translate the sample either manually (via a joystick) or in an automated way using the Lab-View software. In addition, a piezo-electric z-stage is essential for focus stabilization or precise z-positioning of the sample.

The focus stabilization is achieved by monitoring the position of a near-IR laser beam, which totally internally reflects from the glass-sample interface, and the reflected beam is monitored on a quadrant photodiode (QPD). Any change in the position of the laser on the QPD corresponds to a change in the z-position, which is corrected via an active feedback loop.

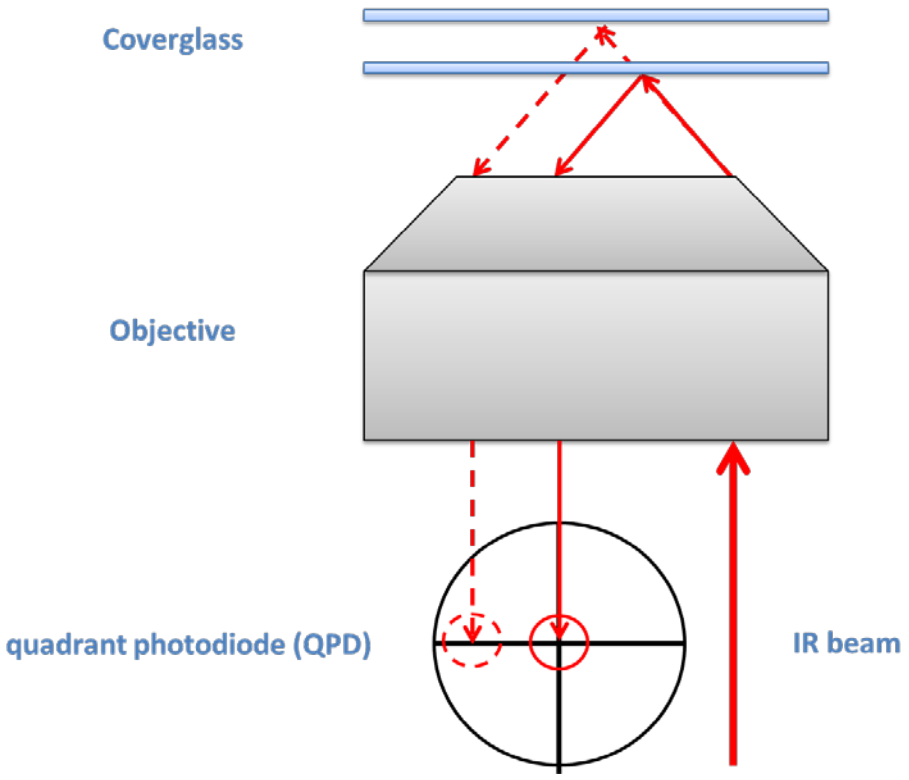

Figure 11 The geometry of the focus lock system. An infra-red laser beam is projected through the objective lens and reflects off the bottom of the sample on the coverglass and back through the objective where its position is detected on a quadrant photodiode (QPD).

The fluorescence light emited by the sample passes through an emission filter and is projected onto an EMCCD camera. Since STORM and PALM rely on the detection of individual fluorescent molecules, the detector of the microscope must have high quantum efficiency in detecting the emitted photons. For this reason an EMCCD is used in our microscope as a detector.

3.2. Material preparation

The sample preparation methods we used in this thesis are described in this section.

3.2.1. Cleaning the coverslip

It is important that the microscopy slides and coverslips used in fluorescence microscopy procedures are extremely clean [32]. We followed the steps below to remove fluorescent contaminants:

1. Fill the beakers with pure water, and place the slides and coverslips into the container separately.
2. Put drops of detergent.
3. Submerge the beakers and sonicate for 15minutes.
4. Rinse under running tap for five minutes. Drain water and repeat the tap water rinse two more times.
5. Repeat sonication in water for another 15 minutes.
6. Decant the water, and sonicate in potassium hydroxide (KOH).
7. Separate coverslips one by one and dry with clean N_2 in a dust free environment.

The slide or coverslip are ready for use in fluorescence experiments after this procedure.

3.2.2.Beads

We use PS-Speck microsphere beads (Molecular Probes' PS-Speck™ Microscope Point Source Kit (P7220)) with a diameter of 0.175 ± 0.005 μm as a control sample. Each suspension has a density of $\sim 3 \times 10^9$ beads/mL. Concentration of beads was determined by using NanoDrop® spectrophotometer. The bead sample preparation is as below:

1. Dilute the beads with water at $1{:}10^5$ to get a low enough concentration in order to lower the probability of beads overlapping in fluorescence images.
2. Add a small drop on the microscope slide.
3. Air dry and protect it from dust during drying.

4. Make a flow chamber by attaching a coverglass to the microscope slide via double sided tape and add water to the flow chamber prior to imaging.

3.2.3.Cyanine Dye 3 (Cy3)

Cyanine dyes are commonly used as fluorescent labels for proteins, nucleic acids and small molecules. Cyanine Dye 3 (Cy3) fluoresces yellow-green with the excitation peak at 550 nm and the emission peak at 570nm. Cy3 can be used as an alternative to Alexa Fluor 555, DY-550, Rhodamine Red-X and TAMRA [5(6)-Carboxytetramethylrhodamine] [33]. In STORM imaging, it can be used as an activator of Cy5 or Alexa 647 fluorescence. In these experiments we used single Cy3 immobilized on glass to produce a sample in which the molecular dipole is fixed and randomly distributed. The sample preparation is as below:

1. Dilute the Cy3 molecules with water at $1{:}3*10^5$ to get a low concentration in order to lower the probability of overlapped molecules in fluorescence images.
2. Add a small drop of diluted Cy3 on the coverglsss and wait for air dry. Pay attention to protect it from dust during drying.
3. Make a flow chamber by attaching the Cy3 containing coverglass to a microscope slide by double sided tape.
4. Add imagine buffer to the flow chamber before imaging.

Concentration of Cy3 was determined by using NanoDrop® spectrophotometer.

3.2.4.Cy3 labelled antibodies

To test the effect of molecular dipole orientation on localization accuracy in STORM, we used an *in vitro* sample in which Cy3 labelled secondary antibodies were immobilized on glass. The first step aimed to label secondary antibodies with Cy3 at a ratio lower than 0.5 Cy3s per antibody. This low labelling ratio was chosen to minimize the possibility of more than one Cy3 molecule on the same antibody. For antibody labelling we used NHS-ester modified Cy3, which can react with the amine groups on

the lysine residues of the antibody. The protocol that we followed was developed at Harvard University in the lab of Prof. Xiaowei Zhuang:

1. For labelling, dissolve one aliquot of Cy3 in 20µL of anhydrous DMSO.
2. Set up labelling reaction with 50µL Donkey-anti-Rabbit (1.3mg/mL), 6µL 1M NaHCO3 (FW 84.01, dissolved in 100µL PBS) and 1.5µL Cy3 (of 20µL aliquot).

   Wrap the tube in aluminium foil to protect from light.

   Allow the reaction to proceed for up to around 40 minutes at room temperature (RT) on a rocking platform with the speed of 73.
3. While the reaction is processing, equilibrate a Nap-5 size exclusion column, one per labelling reaction.

   Run three column volumes of PBS through the column.
4. After the incubation, stop the reaction by the addition of 140µL of PBS to bring the reaction volume up to 200µL (the minimum column loading volume) and gently vortex.

   Add the entire volume to the centre of the column.
5. Allow the sample (130µL) to enter the column and after the last drip add sufficient PBS to collect the fastest running colored band.
6. Add 300µL PBS and collect the resulting eluent in a 1.5mL Eppendorf tube.
7. Store the antibody at 4℃ protected from light, for up to 6 months.
8. Calculate the antibody concentration and labelling ratios by using the NanoDrop.

   In this case, we got the ratio of 0.4239 Cy3 per antibody.

The labelled antibodies were used *in vitro* for the localization error measurements. However, to simulate conditions as close as possible to the cellular labelling using these antibodies, we first attached primary antibody (Rabbit IgG) to the coverglass at a high concentration. We then used blocking buffer (containing BSA) to block the non-specific sticking of the secondary antibody to glass [34]. After washing, Cy3 labelled secondary antibody with a concentration of 0.42 dyes per antibody was introduced and bound to the primary antibody. Figure 12 shows this preparation.

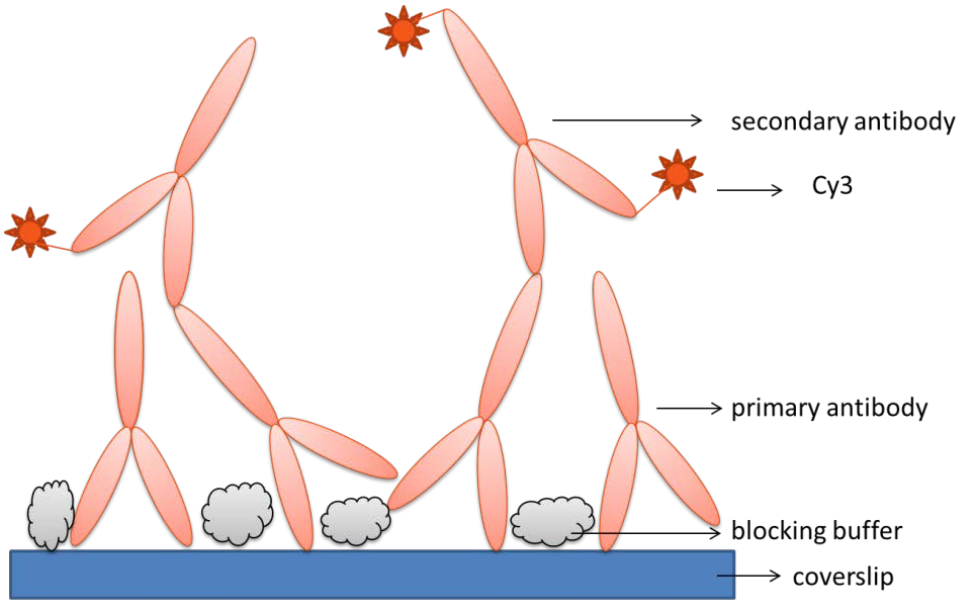

Figure 12 Scheme of Cy3 labelled antibodies

The detailed protocol is as follows:

1. Dilute the primary antibody in water at 1:1000.
2. Load into a flow chamber made from a standard coverslip, a microscope slide and double-sided tape, and incubate for 30 min.
3. Rinse the chamber by blocking buffer to prevent non-specific binding of secondary antibodies to the glass, and incubate for 1 hour.
4. Dilute the secondary antibodies with water at 1:10000 to get a much lower concentration than primary antibody and prevent overlapping spots in fluorescence images.
5. Introduce into the flow chamber and incubate for 5 minutes.
6. Rinse with water.
7. Flow in imaging buffer (MEA 1% and GLOX 1% used as an oxygen-scavenger that removes oxygen from the medium to reduce photobleaching [35])

Concentration of antibodies was determined by using NanoDrop® spectrophotometer.

We found that our samples (either with or without the antibleach solution) can be kept at 4ºC for a day's worth of imaging.

3.3. Experimental design

This thesis aims to characterize the effect of molecular dipole orientation on the resolution of super-resolution fluorescence microscopy techniques that rely on single molecule detection and localization (see Chapter 1 and Chapter 2). The idea is that if the molecular dipole has an axial component with respect to the focal plane, it will be mis-localized when it is out of focus. Engelhardt et al. demonstrated this for molecules that are fixed onto a glass surface, by scanning the piezo stage between -300 and +300 nm and localizing their position in each frame during the scan. They found displacements as large as >200 nm between the position of the molecule at +300 and -300 nm. They attribute this displacement to the errors in localization due to the effect of molecular dipole orientation. They eliminate any error from stage drift by measuring the position of the same molecule in the focal plane twice (in the beginning and at the end of the scan) and make sure that these two measurements give similar positions [30].

In our experiments, however, we found that the stage drift was larger than the Engelhardt et al. paper. In addition, we noticed that any misalignment that could lead to optical distortions (such as astigmatism) could also affect the results. Finally two molecules overlapping within the same diffraction limited volume could also bias the results. Therefore to minimize errors due to stage drift, optical distortions and overlapping molecules, we designed our experiments slightly differently from the Engelhardt et al. paper [30].

The Labview data acquisition software chooses one peak in a certain region randomly given that its intensity is higher than the threshold we set in advance. This selected spot is then centred in the field of view by automatically translating the *xy*-stage. This peak is then imaged for 40 frames, flipping between two different *z* positions (e.g +300 nm and

-300 nm), 20 frames for each position. At the end of 40 frames the stage returns to the focal plane (z=0 nm), and imaging continues there until the molecule is photobleached.

The next sections describe how this experimental design helps us minimize errors from optical distortions, stage drift and multiple overlapping molecules in more detail.

3.3.1. Peak selection

A home-made microscope system can suffer from optical distortion due to small errors in alignment. The effect of optical distortion such as astigmatism can be different for the different regions of the field of view (FOV). For example the optical distortions can be worse along the edge of the FOV compared to the centre. In order to keep the conditions such as the amount of optical distortion constant for all the molecules, we analyse only one single molecule that is placed in the centre of the field of view each time, instead of the whole field of view.

For further eliminating the effect from optical distortion, we first test PS-Speck microsphere beads (Molecular Probes' PS-Speck™ Microscope Point Source Kit (P7220)). Since these beads are uniformly coated with many fluorophores, they should represent an isotropic point source in terms of molecular dipole orientation. We localized the position of these beads by flipping between two different focal planes as described previously and assume that any displacement in the positions between these two focal planes is a result of optical distortions. By finding the average displacement over all beads in x, y, we could determine the displacement due to optical distortions, which we then used as a correction factor in single molecule experiments. The details are described in section 4.

3.3.2. Flipping

The sequential flipping between two focal planes (for example +300 and -300 nm), rather than doing one scan starting from +300nm and finishing at -300nm [30] was designed to minimize errors due to stage drift, which can be difficult to correct for

properly. In practice, in order to minimize the effect of stage drift, we keep the sample on the focal plane several minutes before starting experiment, and also put some weight on the sample. However, stage drift is unavoidable and therefore our flipping experiment is designed to restrict the effects of stage drift on the measured positions to only the drift between two consecutive frames (see Figure 13). Given that our exposure time is 0.1s, the drift between two consecutive frames should be rather small. Figure 13 demonstrates that any effect due to stage drift will be limited to that between two consecutive frames in a "flipping" experiment.

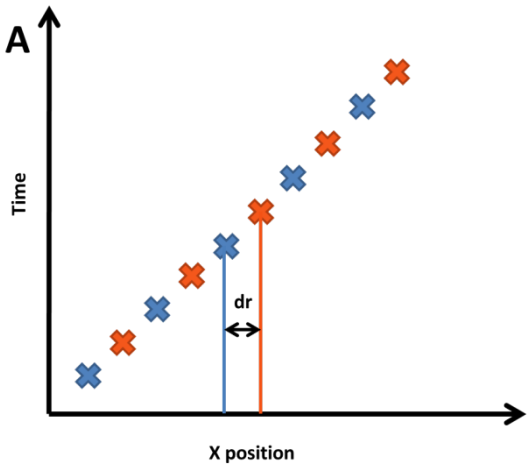

Figure 13 The effect of stage drift on the measured position. The red crosses represent the consecutive *x* location of the same molecule at *z*=+200nm, while the blue ones represent the consecutive x position of that molecule at z=-200nm. The positions are measured one after the other by flipping the piezo stage between z=+/-200 nm. We assume that the molecule's position at +/-200 nm is the same and any shift in position is due to a linear stage drift. The blue line and the red line represent the average measured position at z=-200 nm and z= +200 nm respectively. As can be seen from this figure, the shift between the measured average positions is equal to the amount of drift between two consecutive frames, which is much smaller than the total drift over the entire experiment duration

3.3.3. Bleaching

The final consideration that we took into account was the effect due to multiple molecules overlapping within a single diffraction limited volume. We tried to minimize overlap by using low Cy3 and low antibody concentrations, to get to a single molecule

density. However, even under these conditions it is possible that two molecules overlap and give rise to errors in the position measurement. In addition, free floating florescent molecules that can pass over the measured molecule will give rise to errors.

We address these problems by evaluating the intensity-time trace of each measured molecule. After the flipping experiment is over, the stage automatically goes back to the focal plane and the fluorescence is recorded until the average intensity of last 10 frames is lower than a pre-set value of background. The intensity-time trace of a single molecule should contain a single stepwise photobleaching event. We can therefore eliminate traces that are not from single molecules or that have contamination from free floating molecules by evaluating their intensity-time traces.

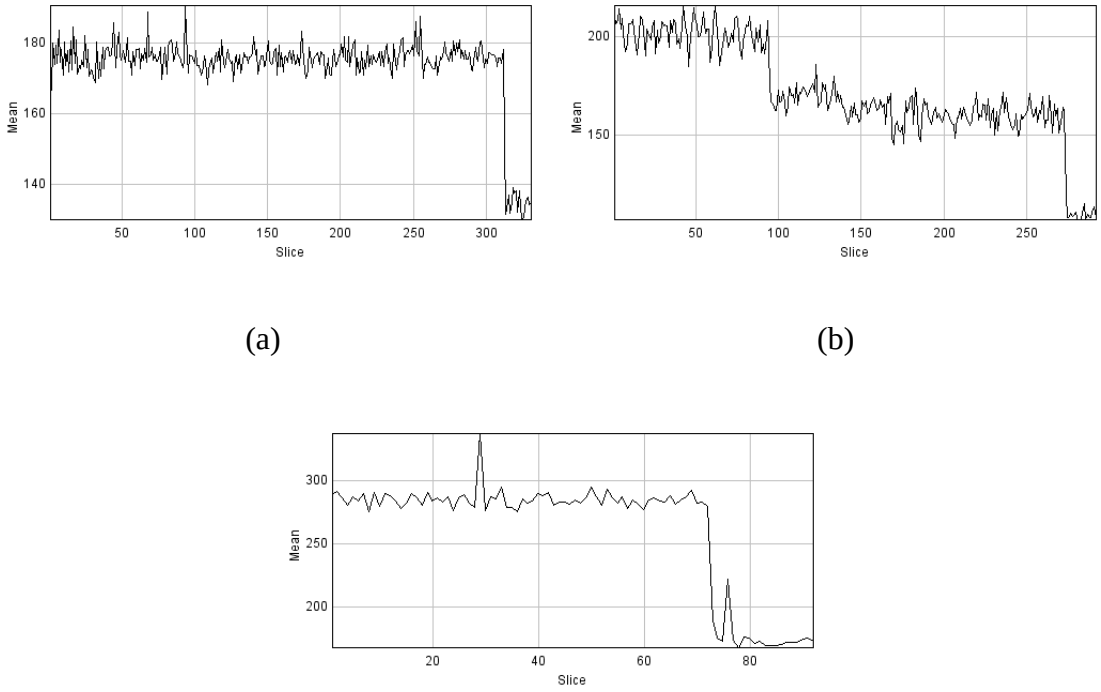

Figure 14 Example of typical intensity trace for the image peaks. (A) shows a clear single step of photobleaching. (B) shows the trace with two photobleaching steps. (C) shows a single-step photobleaching with two high intensity spikes.

Figure 14 shows examples of different traces that we could observe in these experiments. Figure 8a shows a trace with a single photobleaching step as would be expected from a single molecule. Figure 8b on the other hand shows a molecule with two photobleaching steps in its trace, likely due to two overlapping molecules within the same spot. Figure 8c shows a molecule that contains “spikes” in its trace, likely due to another molecule floating over this molecule in that frame. We exclude traces with multiple steps or with spikes from our analysis and only keep those traces that show a single photobleaching step without any spikes.

3.4. Data analysis procedure

3.4.1. Software used

We rearrange the order of imaging using an ImageJ macro to group the frames with the same *z* position together. We then use a Java script to fit the peak to a Gaussian and extract information such as *x*, *y* position, intensity, background, frame number, peak number and *x*, *y* standard deviation of the Gaussian fit. After getting these raw data, we use Excel and Origin to correct the optical distortion.

A square region of 5×5 pixels which we call box size is centred on each peak, which is in the centre of field of view with 256×256 pixels. 5×5 pixels is ideal for the diffraction limited spot size in our experiments. A too large of a box size could potentially include the adjacent fluorescent molecules which in turn will lower localization precision. At the same time, a too small of a box size would exclude photons and lower the localization precision.

A single molecule emitter, which is typically much smaller than the diffraction limit, can be treated as a point source. Therefore, a two dimensional Gaussian function is used to fit to the data for determining the peak centre position, amplitude, and width:

$$I(x,y) = A_0 + I_0 e^{-\frac{1}{2}\left[\left(\frac{x-x_0}{\sigma}\right)^2+\left(\frac{y-y_0}{\sigma}\right)^2\right]}$$

where A_0 is the background fluorescence level, I_0 is the amplitude of the peak intensity profile, x_0 and y_0 are the centre coordinates of the peak, and σ is the standard deviation of the Gaussian profile of the peak [3]. The total number of counts collected in the peak, which is calculated as $2\pi\sigma^2 I_0$, is converted to photoelectrons using the preset EMCCD conversion factor, which in turn gives the number of photons detected.

3.4.2. Correction methods

After the Gaussian fitting, we obtain the *x* and *y* positions of each peak at two different focal planes (e.g. +300nm and -300nm). We calculate the average of *x* and *y* position for each peak at the two focal planes of -300nm and +300nm, respectively, and define the total original displacement as: $dr = \sqrt{dx^2 + dy^2}$, where dx is the difference of average *x* at two *z* planes, and dy is the difference of average *y* at two *z* planes. This displacement will give us the error in localization accuracy with respect to the focal plane

The PS-Speck microsphere beads (Molecular Probes' PS-Speck™ Microscope Point Source Kit (P7220)) we used are isotropic and uniform, so the displacement between the different *z* positions should be within our localization error (~8.2 nm) in theory. However, in practice, from the result (see section 4) this is not the case, likely due to the optical distortions, such as astigmatism.

In order to correct errors that are independent of molecular orientation such as optical distortions, we averaged dx and dy over all the beads and defined the corrected displacement of molecules as below:

$$dr_{corrected} = \sqrt{(dx - x_{distortion})^2 + (dy - y_{distortion})^2}$$

where dx once again is the difference of average x at two z positions for a given molecule and $x_{distortion}$ is the optical distortion in x calculated by averaging the displacement in x (dx) over all beads.

3.4.3. Filter

We manually filtered out the molecules with multiple-steps or high spikes in the first 40 frames of their intensity-time traces, and only keep the one with single step in the final results as we discussed before in 3.3.3.

Chapter 4 Result and discussions

In this chapter, we will show the results for the measurement of localization displacement on *x,y* positions of the same molecule at two different z-positions caused by molecular dipole orientation.

We measured not only Cy3 immobilized on the glass, but also Cy3 labelled antibodies so as to simulate the similar condition as real STORM imaging.

In order to get rid of the other possible sources of localization displacement, we used PS-Spaeck beads as a uniform emitter, which allowed us to correct for optical distortions. In addition we looked at intensity-time traces of Cy3 molecules and only used those molecules whose traces contained a single photobleaching event (see section 3.2.4).

All the experimental and material preparation methods are described previously in Chapter 3.

Figure 15 shows an example of the type of data we obtained after analysis and appropriate corrections have been applied. These examples were chosen from Cy3 labelled antibodies. In blue is plotted the x-position (Figure 15(a) and Figure 16(a)) and y-position (Figure 15(b) and Figure 16(b)) of the same molecule in one focal plane (-200nm) in 20 separate measurements. Similarly in red are the positions obtained in the second focal plane (+200nm). The blue line is the average position (averaged over the 20 results) in one focal plane and the red line is the average position in the other focal plane. Since we made a big effort to correct for optical distortions, the displacement in the average positions is most likely due to mislocalization of the molecule as a result of a tilt in its molecular orientation. Figure 15(c) is the *x* and *y* positions plotted together in one or the other focal plane. This particular molecule did not show a large displacement in its average position between the two focal planes. Figure 16 shows an example molecule that had a large displacement in its position between the two focal planes.

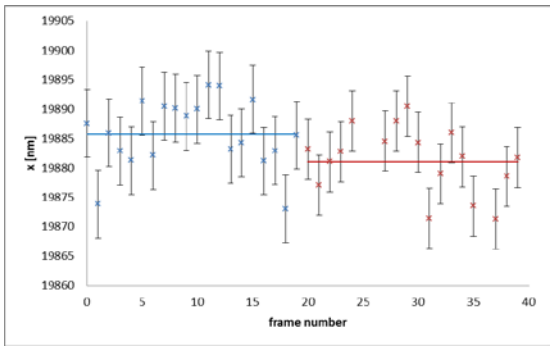

(a)

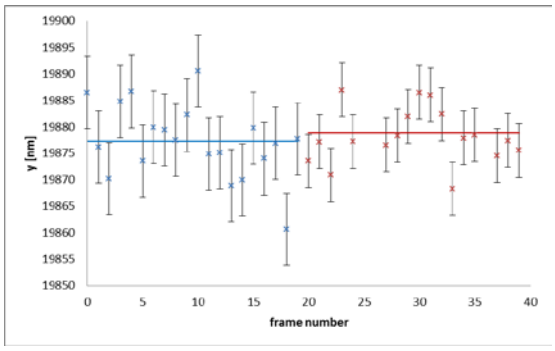

(b)

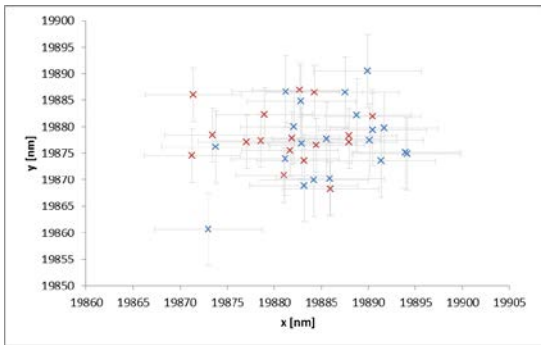

(c)

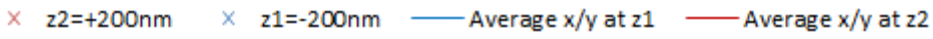

Figure 15 Example of localization track for a single Cy3 molecule attached to an antibody: Molecule shows only a small displacement in its position between the two focal planes. (a) and (b) show the *x* and *y* positions separately obtained in each frame at +200 nm and -200 nm . Each focal plane is imaged for 20 frames and the molecule is localized once in each frame. The average of the 20 frames is given by the blue and red lines. Two clusters at two focal planes can be seen in (c). Here, *dx*=4.68725nm, *dy*=-1.6512nm, *dr*=4.969584892nm, corrected *dx*=-3.598860479nm, corrected *dy*=0.675327695nm, and corrected *dr*=3.661675059nm.

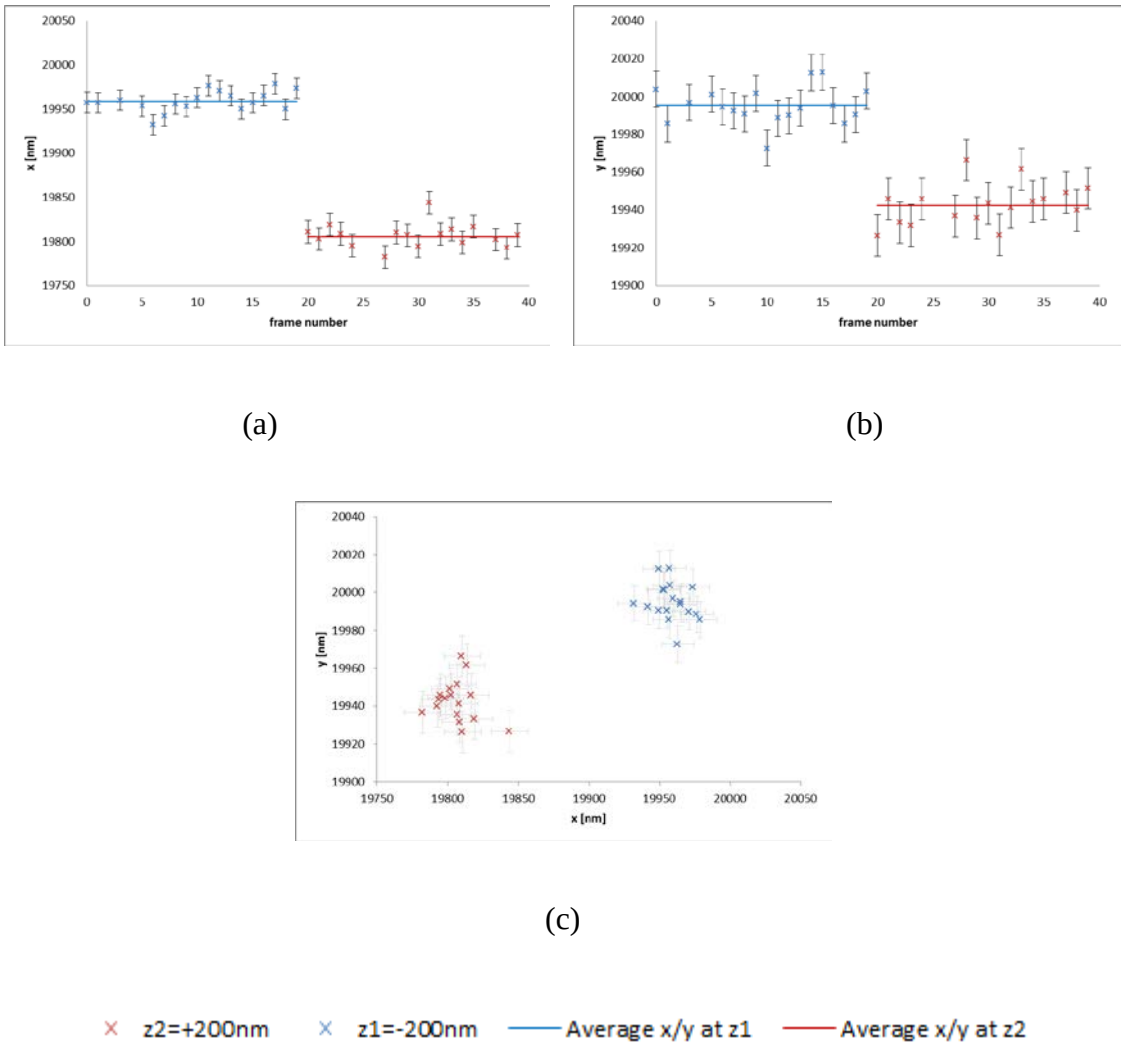

(a) (b)

(c)

Figure 16 Example of localization track for a single Cy3 molecule attached to an antibody: Molecule shows a large displacement in its position between the two focal planes. Here, *dx*=153.2079111nm, *dy*=52.8798nm, *dr*=162.0769486nm, corrected *dx*=152.1236327nm, corrected *dy*=26.44352169nm, and corrected *dy*=154.4048557nm.

4.1. Results from the PS-Speck beads

We used the PS-Speck microsphere beads (Molecular Probes' PS-Speck™ Microscope Point Source Kit (P7220)) with a diameter of 0.175 ± 0.005 µm, as an isotropic point source. These beads have excitation and emission peaks at 540nm and 560 nm respectively.

We analyzed many beads positioned in the center of the field of view and determined their positions at multiple focal planes (±100nm, ±200nm and ±300nm). We only included those beads in our analysis whose intensity was within the intensity range for a single bead. Few beads showed intensities much higher than what would be expected from an individual bead and those were excluded from the analysis. Before correction for optical distortion, the average of total displacement *dr* in the position of PS-Speck beads between two focal planes was found to be 5.0375nm, 9.8751nm and 13.2907nm for focal planes of ±100nm, ±200nm and ±300nm, respectively (see Table 1). Since the beads are uniform and isotropic, there should be no contribution to the displacement in position between different focal planes from the molecular dipole orientation. As a result, in principle the displacement should be within the localization precision, however we find the displacement to be slightly larger than expected. This is likely die to optical distortions of the microscope set up, such as astigmatism.

	Optical distortion (nm)		Correction (nm)	
	Average of dx	Average of dy	Original displacement	Corrected displacement
±100nm (based on 79 beads)	4.036244937	1.761736709	5.037468424	2.788276133
±200nm (based on 61 beads)	8.286110479	-2.326527695	9.875084763	3.93921064
±300nm (based on 93 beads)	11.27669788	4.433182381	13.29067884	5.810459525

Table 1The result for beads measured in different z positions.

As previously explained, we used the average displacement in *x*, and *y* (averaged over many beads) to correct for these optical distortions. Enough statistics (79 beads for ±100nm, 61 beads for ±200nm and 93 beads for ±300nm) are collected to determine the average displacement in *x*,*y* (average of *dx* and *dy*) to correct for effects not related to molecular dipole orientation.

After subtracting this correction factor from the displacement of individual beads the average corrected displacement of PS-Speck beads reduced to 2.7883nm, 3.9392nm and 5.8106nm for z position of ±100nm, ±200nm and ±300nm, respectively (Table 1).

While the correction improved the results, it did not completely eliminate the displacement in the bead positions between multiple focal planes, especially when the focal planes were separated by large distances (+/-300 nm). The remaining displacement is due to our inability to fully correct for all distortions and therefore demonstrates the remaining error that is due to effects other than molecular dipole orientation (see Figure 17). The residual error is very small.

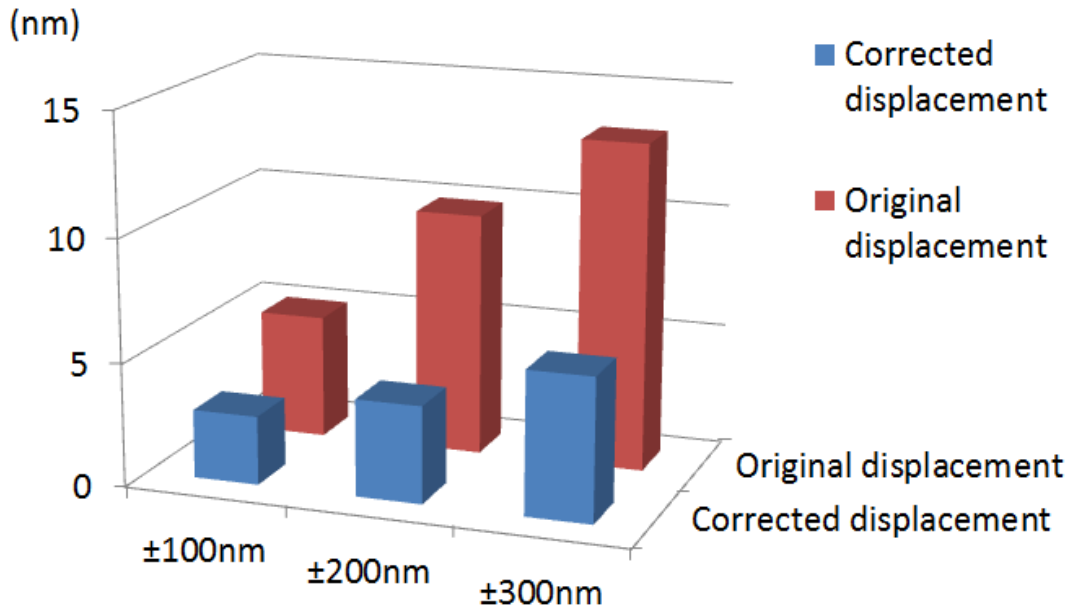

Figure 17 Compare the original displacement and corrected displacement in different z positions.

4.2. Results from molecules (Cy3) that have been fixed onto coverglass

We immobilized Cy3 molecules onto a cover glass at low concentration such that we could image single molecules. Cy3 was attached to the coverglass through electrostatic interactions. This attachment in principle should generate a fixed molecular dipole orientation and the orientation (and the tilt angle) of the different Cy3 molecules should in principle be randomly distributed. We selected Cy3 because it is bright and is commonly used as a fluorescent label.

Since the measured molecules are randomly oriented the displacements measured (dx and dy) over many molecules after correction for optical distortions should follow a uniform distribution around 0 nm. The distribution of Cy3 displacements *dx* and *dy* between z=±200nm after correction for distortions is shown in Figure 18 and Figure 19.

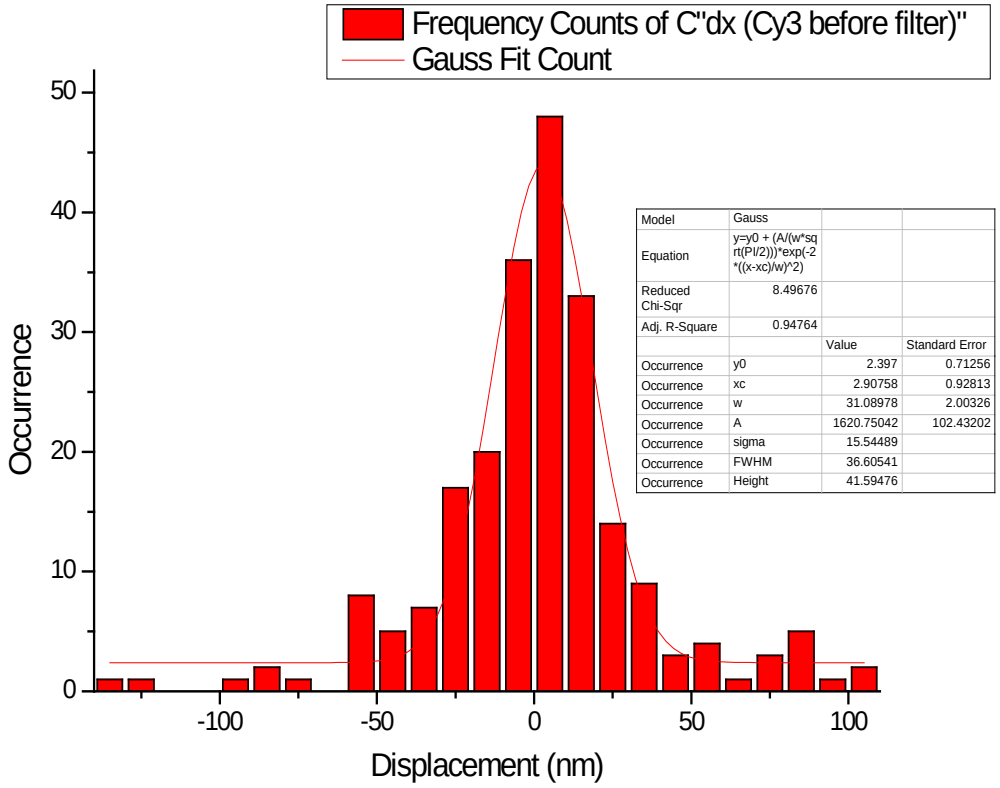

Figure 18 Histogram of displacement *dx* of Cy3 measured at z=+200nm and -200nm before filter (222 statistics). The center of Gaussian fitting is 2.90758nm.

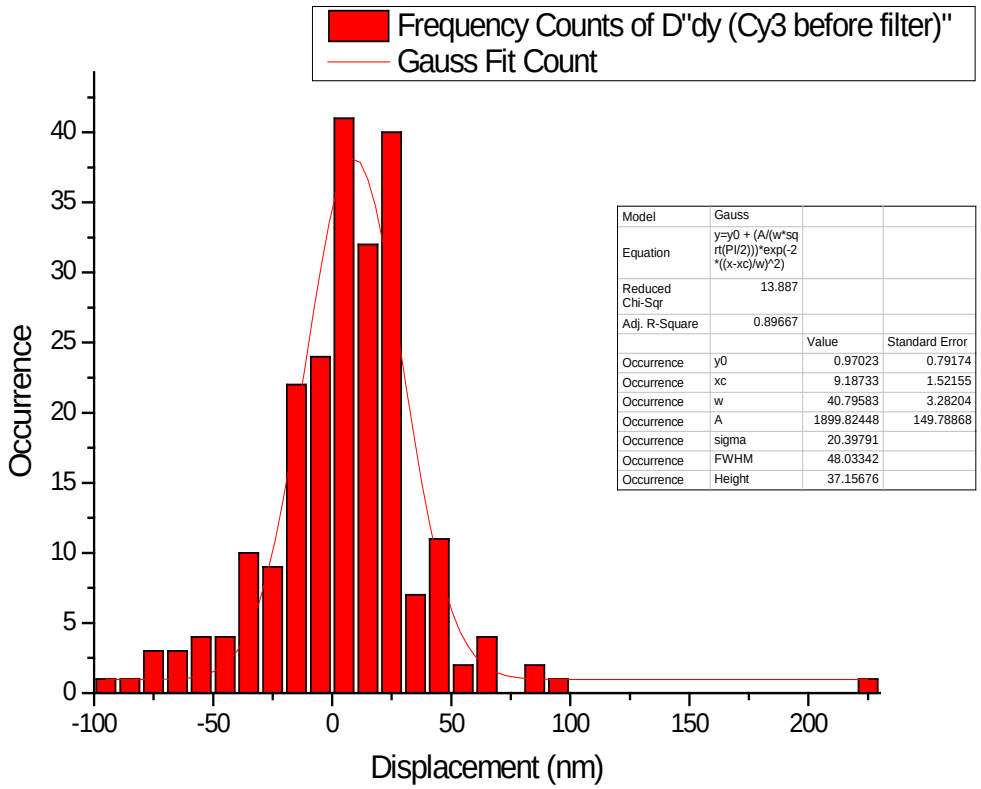

Model	Gauss		
Equation	y=y0 + (A/(w*sqrt(PI/2)))*exp(-2*((x-xc)/w)^2)		
Reduced Chi-Sqr	13.887		
Adj. R-Square	0.89667		
		Value	Standard Error
Occurrence	y0	0.97023	0.79174
Occurrence	xc	9.18733	1.52155
Occurrence	w	40.79583	3.28204
Occurrence	A	1899.82448	149.78868
Occurrence	sigma	20.39791	
Occurrence	FWHM	48.03342	
Occurrence	Height	37.15676	

Figure 19 Histogram of displacement *dy* of Cy3 measured at z=+200nm and -200nm before filter (222 statistics). The center of Gaussian fitting is 9.18733nm.

The distribution of displacements in x and y axis indeed showed a uniform distribution around zero.

Among these molecules, we filtered out those whose intensity-time traces did not show a single photobleaching step. After this filter the remaining distribution of total displacement dr between focal planes +/-200 nm after correction for distortions is shown in Figure 18. After correction, the average of total displacement was around 39.6296nm. We expected to obtain a uniform distribution with a large range since the tilt angle of the molecules should be randomly distributed and fixed. However the distribution of total corrected displacement showed a peak around 20 nm. This could be due to several factors:

The tilt angles may not be completely random as the molecule may have a preferred orientation when it becomes fixed onto the flat surface of the glass substrate. In addition, it is possible that those molecules that have a large tilt angle are much dimmer than molecules with smaller tilt angles, and are preferentially picked in our experiments and analyzed in the final data, therefore biasing the results towards a certain displacement. In addition +/-200 nm may not be a large enough focal shift to fully determine the effect of error in position measurement due to molecular orientation. As a result, we next examined the displacement in position between focal planes +/-300nm.

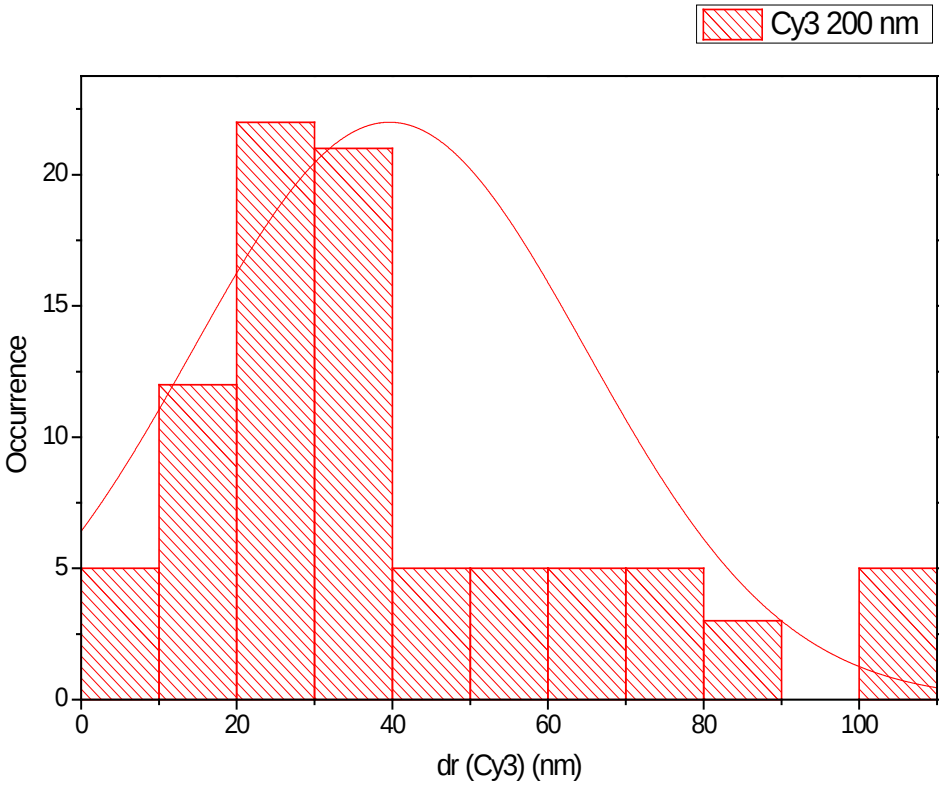

Figure 20 Average total corrected displacement of Cy3 measured between z-position ±200nm (based on 88 molecules).

The distribution of corrected total average displacement showed a larger range when measured between +/-300 nm (up to 180 nm displacement could be measured). The distribution obtained from 34 molecules also looked more uniformly distributed,

however more statistics are needed to make a full conclusion about the shape of the distribution. The average corrected displacement for +/-300 nm was 80.0608nm.

These results confirm that, if the molecules cannot rotate freely, the centroids of their positions determined at different focal planes will contain a large displacement because there will be a large error in determining their coordinates.

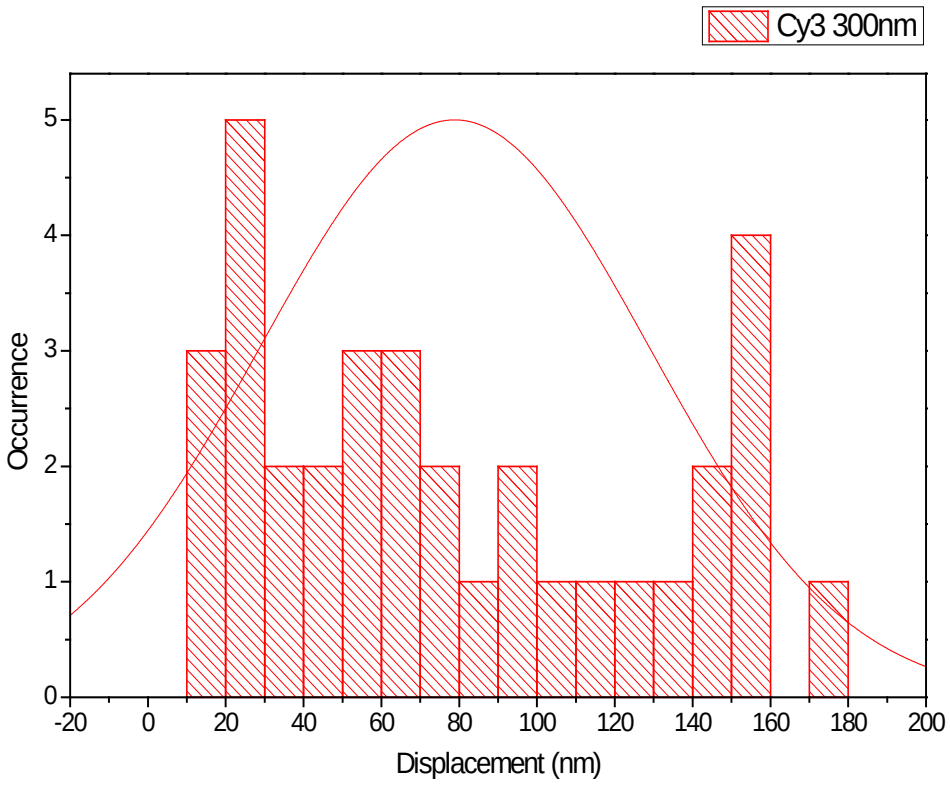

Figure 21 Average total corrected displacement of Cy3 measured between z-position ±300nm (based on 34 molecules).

In their paper, Engelhardt et. al. [30] measured a similar range of displacements in the mean positions of a different molecule (perylene) when measured at different focal planes spanning a range between +/-300 nm. Our results therefore are in agreement with their results.

4.3. Results from Cy3 labelled antibodies

While the Cy3 molecules fixed on coverglass provide an initial characterization of the errors that can result due to molecular orientation, they do not reflect the conditions in a real STORM experiment. We aimed to create an *in vitro* protocol that resembled most closely the sample preparation used in STORM imaging. For this purpose we attached primary antibodies onto coverglass and used Cy3 labeled secondary antibodies to target the primary antibodies (see section 3.2.4).

To make sure that the movement of antibodies themselves do not introduce any errors we first determined the displacement in the position of a single Cy3 molecule measured at the same focal plane (z=0) multiple times. We recorded 40 frames of Cy3 molecules in the focal plane and determined the position in each frame. We then split the positions between the first and last 20 frames and determined the average position by averaging over these initial and final 20 frames. We defined the displacement to be the difference between these average positions. When the focal plane was kept constant the average displacement was small (4.4956 nm) indicating that there are no errors due to any possible motion of the antibodies themselves.

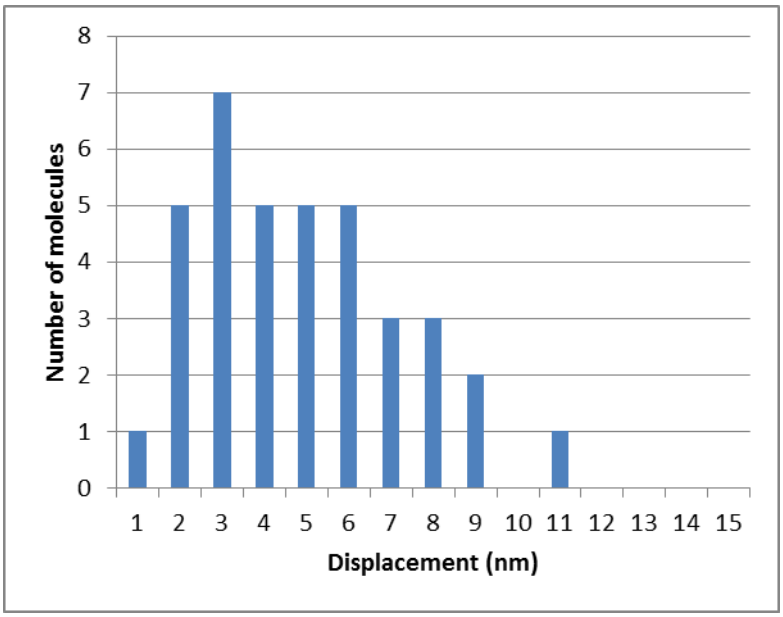

Figure 22 Total displacement in the position of Cy3 labelled antibodies measured at z=0 nm which is based on 37 statistics. The average of displacement is 4.4956nm.

We next repeated the same experiments as in the case of Cy3 molecules immobilized on glass. The distribution of displacements in x and y (dx and dy) of Cy3 labelled antibodies measured at z=±200nm is shown in Figure 23 and Figure 24.The dx and dy was uniformly distributed around 0 nm as expected (Gaussian fitting showed a mean at 4.4966nm and 2.6048nm, and the FWHM of 67.1219nm and 30.4666nm, respectively).

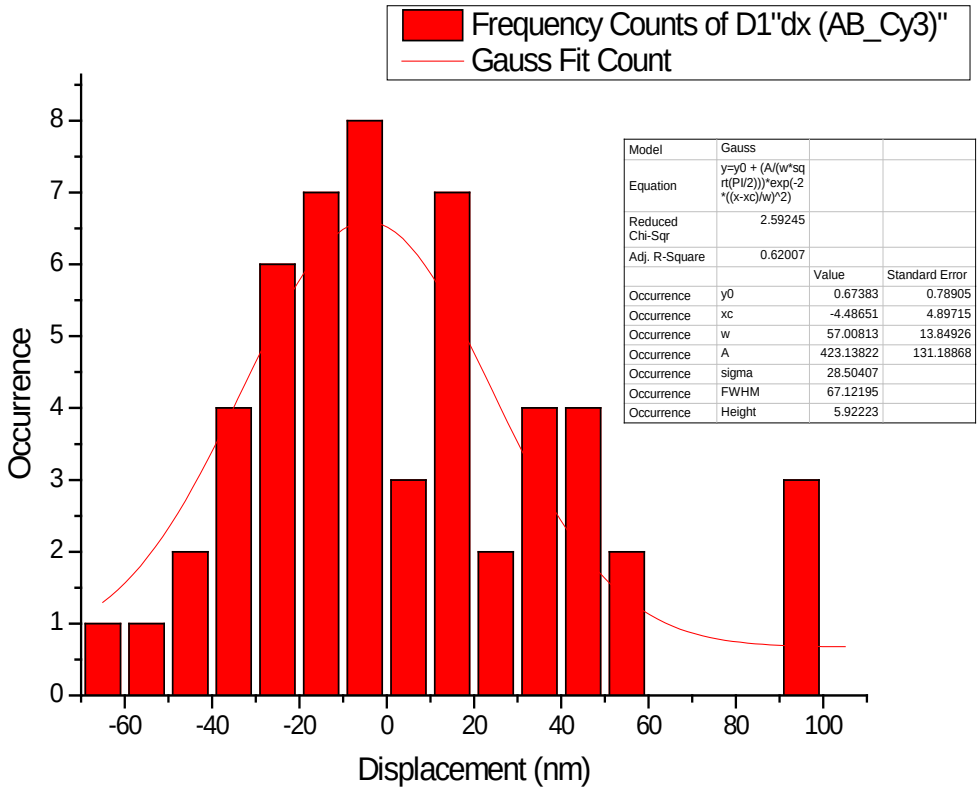

Model	Gauss		
Equation	y=y0 + (A/(w*sqrt(PI/2)))*exp(-2*((x-xc)/w)^2)		
Reduced Chi-Sqr	2.59245		
Adj. R-Square	0.62007		
		Value	Standard Error
Occurrence	y0	0.67383	0.78905
Occurrence	xc	-4.48651	4.89715
Occurrence	w	57.00813	13.84926
Occurrence	A	423.13822	131.18868
Occurrence	sigma	28.50407	
Occurrence	FWHM	67.12195	
Occurrence	Height	5.92223	

Figure 23 Histogram of displacement dx of Cy3 labelled antibodies measured at z=+200nm and -200nm after filtering for single-step photobleaching and after correction for optical distortions (54 statistics). The center of Gaussian fitting is 4.4966nm.

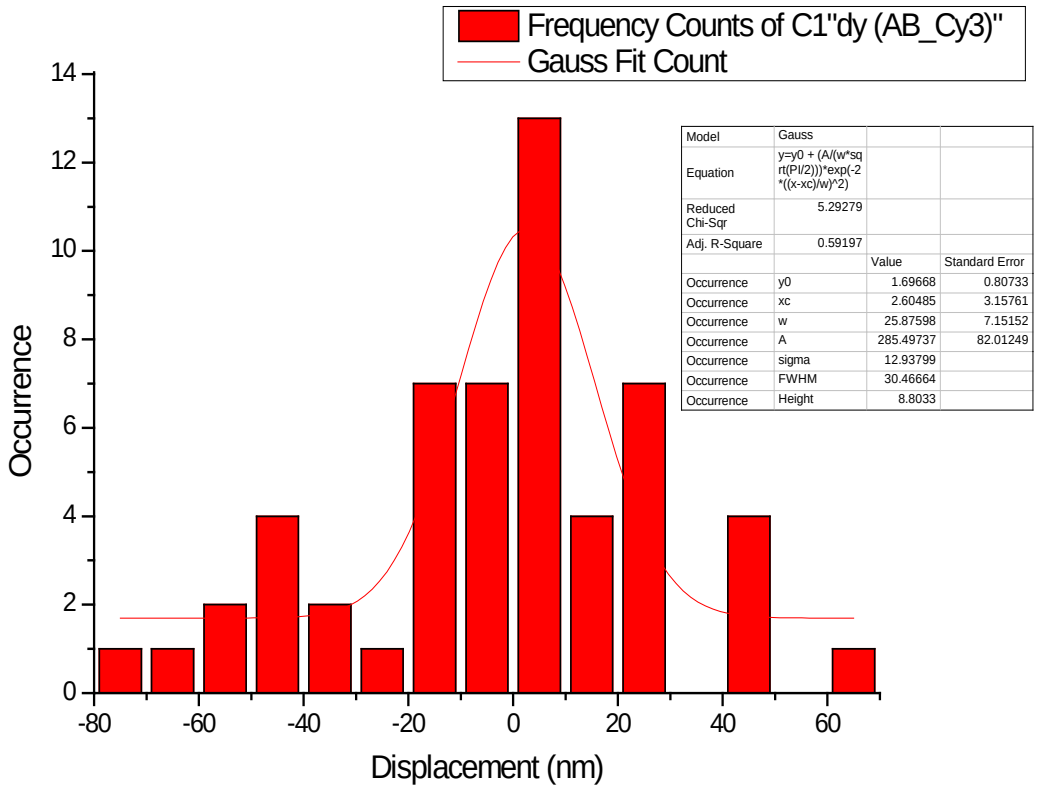

Model	Gauss		
Equation	y=y0 + (A/(w*sqrt(PI/2)))*exp(-2*((x-xc)/w)^2)		
Reduced Chi-Sqr	5.29279		
Adj. R-Square	0.59197		
		Value	Standard Error
Occurrence	y0	1.69668	0.80733
Occurrence	xc	2.60485	3.15761
Occurrence	w	25.87598	7.15152
Occurrence	A	285.49737	82.01249
Occurrence	sigma	12.93799	
Occurrence	FWHM	30.46664	
Occurrence	Height	8.8033	

Figure 24 Histogram of displacement dy of Cy3 labelled antibodies measured at z=+200nm and -200nm after filtering for single-step photobleaching and after correction for optical distortions (54 statistics). The center of Gaussian fitting is 2.6048nm.

The total corrected displacement for Cy3 labeled antibodies measured at z=+/-200nm is shown in Figure 25. After correction, the average of total displacement is around 38.6434nm and spans a range of 110 nm.

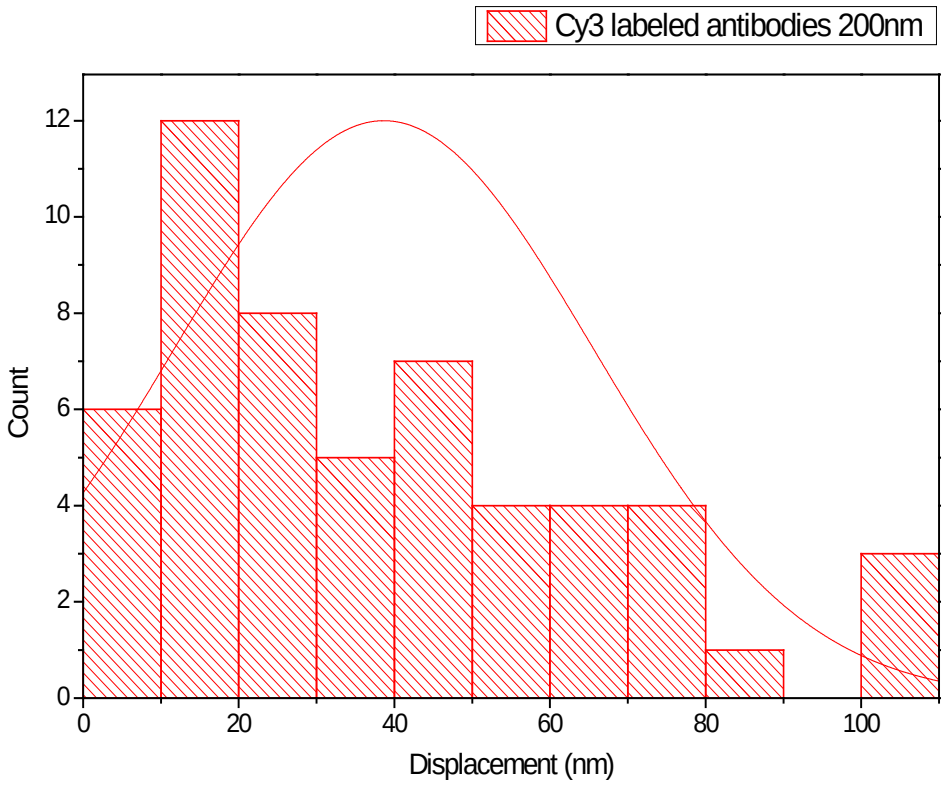

Figure 25 Total corrected displacement of Cy3 labelled antibodies measured at r z=±200nm (based on 54 molecules).

These results are comparable to Cy3 fixed on coverglass, which is surprising. We expected that the flexible linkage of Cy3 to the antibody will provide rotational freedom therefore minimizing any effect due to molecular orientation. However, as mentioned earlier the Cy3 may not get fixed onto coverglass in a completely random manner giving rise to a preferred orientation. In addition since the molecules with lower tilt angles are brighter, this may also bias the results towards those molecules. As a result the Cy3 immobilized on glass may not reflect the ideal randomly distributed fixed molecular orientation case. Further experiments are needed to fully understand the lack of difference between Cy3 molecules fixed to glass and Cy3 molecules attached to antibodies.

Table 2 summarises the results for Cy3 on coverglass and Cy3 labelled antibodies

Corrected average displacement (nm)	Cy3	AB Cy3
+/- 200nm	39.62961206	38.64339422
+/- 300nm	80. 0608561	-----

Table 2 Compare the result between Cy3 and Cy3 labelled antibodies for z=±200nm and ±300nm .

Chapter 5 Conclusions

Super-resolution fluorescence imaging techniques by single molecule approach, such as photoactivated localization microscopy (PALM) [19], fluorescence photoactivation localization microscopy (FPLAM) [20], stochastic optical reconstruction microscopy (STORM) [18], has revolutionized far-field fluorescence imaging in the last decade and opened the door for research on biological and biomedical processes at the nanometer scale. With these techniques, we are now able to see the composition of biological cells with previously unobserved detail at the sub-cellular and molecular level, up to a resolution of 20-30 nm.

However, these kind of techniques are highly dependent on the localization precision and accuracy of individual molecules. Among all those influencing factors of localization precision and accuracy, the dipole molecular orientation can play a significant role in the localization accuracy in STORM and PALM imaging. However the effect of molecular dipole in localization accuracy has not been fully characterized under realistic sample preparation conditions for STORM.

In this thesis, we demonstrate the combined effect of molecular tilt and defocus on localizing the centroid of fluorophores in far-field super-resolution fluorescence microscopy based on single molecule localization.

To study the effect of molecular dipole orientation, we chose to study Cy3, a bright and commonly used synthetic fluorophore. We determined the total average displacement in the mean position of this molecule determined at separate focal planes (e.g. +/-200 nm or +/- 300 nm) under different sample preparation conditions. We used isotropic fluorescent beads to correct for any effects that are not due to dipole orientation (such as optical distortions). We first studied the case of molecules whose orientation has been fixed by attaching them to a glass substrate and found the average total displacement to be 39.6296nm for +/-200nm spanning a range up to 110 nm and 80.0609nm for +/- 300 nm spanning a range up to 180 nm. Due to time limitations we could only determine

the displacement for Cy3 labeled antibodies measured at +/-200 nm and not at +/- 300 nm. We found the average displacement and the total range to be comparable to the Cy3 molecules fixed on glass. This result is surprising since we expect that when the molecules are attached to the antibody they should have some rotational freedom, which should reduce the error in localization accuracy compared to molecules whose orientation are completely fixed. We believe that the reason for this discrepancy is likely due to a biased sampling of the molecules attached to glass. These molecules may not completely randomly orient and may preferentially attach in a way that their dipole is aligned parallel to the optical axis. In addition those molecules that have a large tilt angle with respect to the optical axis may be too dim to be recorded in our experiments.

In conclusion, we find that the dipole orientation of molecule indeed plays a significant role in the localization accuracy in super-resolution fluorescence imaging techniques by single molecule approach even under conditions in which the dye is attached to the antibody with a flexible linker. This error in localization accuracy should directly affect the image resolution. In a simplified scenario, the average total displacement that we measured (~39 nm) can be convolved with the localization precision (~20 nm) therefore leading to a worse effective localization precision. In this case the two errors can be added in quadrature to obtain an effective localization precision of ~43 nm.

Reference

[1] K. R. Spring and M. W. Davidson, "Introduction to Fluorescence Microscopy," NIKON, [Online]. Available: http://www.microscopyu.com/articles/fluorescence/fluorescenceintro.html.

[2] M. Bates, B. Huang and X. Zhuang, "Super-resolution imaging by nanoscale localization of photo-switchable fluorescent probes," *Current Opinion in Chemical Biology*, vol. 12, no. 5, p. 505–514, 2008.

[3] W. M. Bates, "Far-field fluorescence microscopy with spatial resolution beyond the diffraction limit," Harvard University, Cambridge, Massachusetts, 2009.

[4] B. Huang, M. Bates and X. Zhuang, "Super-Resolution Fluorescence Microscopy," *Annual Review of Biochemistry,* no. 78, pp. 993-1016, 2009.

[5] E. K. Abbe, "Beitrage zur Theorie des Mikroskops und der mikroskopischen," *Arch Mikroskop Anat,* no. 9, p. 413, 1873.

[6] B. Hecht,, B. Sick and U. P. Wild, "Scanning near-field optical microscopy with aperture probes:Fundamentals and applications," *The Journal of Chemical Physics,* vol. 112, no. 18, p. 7761–7774, 2000.

[7] H. Stefen and S. EHK, "Confocal microscopy with an increased detection aperture:type-B 4Pi confocal microscopy," *Optical letter,* vol. 19, no. 3, pp. 222-224, 1994.

[8] G. MG, A. DA and S. JW, "I5M:3D widefield light microscopy with better than 100nm axial resolution," *Journal of microscopy,* vol. 195, no. 1, pp. 10-16, 1999.

[9] G. MG., "Surpassing the lateral resolution limit by a factor of two using structured illumination microscopy," *J Microsc,* vol. 198, no. 2, pp. 82-87, 2000.

[10] S. Hell and J. Wichmann, "Breaking the diffraction resolution limit by stimulated emission: stimulated-emission-depletion fluorescence microscopy,"

Optics Letters, vol. 19, no. 11, p. 780–782, 1994.

[11] T. A. Klar and S. W. Hell, "Subdiffraction resolution in far-field fluorescence microscopy," *Optics Letters*, vol. 24, no. 14, p. 954–956, 1999.

[12] B. Harke, J. Keller, C. K. Ullal, V. Westphal, A. Schönle and S. Hell, "Resolution scaling in STED microscopy," *Optics Express*, vol. 16, no. 6, pp. 4154-4162, 2008.

[13] T. A. Klar, S. Jakobs, M. Dyba, A. Egner and S. Hell, "Fluorescence microscopy with diffraction resolution barrier broken by stimulated emission," *Proc. Natl. Acad. Sci. U. S. A.*, vol. 97, no. 8206, 2000.

[14] D. Wildanger , R. Medda , L. Kastrup and S. Hell, "A compact STED microscope providing 3D nanoscale resolution," *Journal of Microscopy*, vol. 236, no. 1, p. 35–43, 2009.

[15] R. E. Thompson, D. R. Larson and W. W. We, "Precise nanometer localization analysis for individual fluorescent probes," *Biophysical Journal*, vol. 82, no. 5, p. 2775–2783, 2002 May.

[16] J. Lippincott-Schwartz and G. H. Patterson, "Photoactivatible fluorescent proteins for diffraction-limited and super-resolution imaging," *Trends in Cell Biology*, vol. 19, no. 11, pp. 555-565, 2009.

[17] M. Fernandez-Suarez and A. Ting , "Fluorescent probes for super-resolution imaging in living cells," *Nat Rev Mol Cell Biol.*, vol. 9, p. 929–943, 2009.

[18] M. J. Rust, M. Bates and X. Zhuang, "Sub-diffraction-limit imaging by stochastic optical reconstruction microscopy (STORM)," *Nature Methods*, vol. 3, no. 10, pp. 793-795, 2006.

[19] E. Betzig, G. H. Patterson, R. Sougrat, O. W. Lindwasser, S. Olenych, J. S. Bonifacino, M. W. Davidson, J. Lippincott-Schwartz and H. F. Hess, "Imaging intracellular fluorescent proteins at nanometer resolution," *Science*, vol. 313, pp. 1642-1645, 2006.

[20] S. T. Hess, T. P. K. Girirajan and M. D. Mason, "Ultra-high resolution imaging

by fluorescence photoactivation localization microscopy," *Biophys J.,* vol. 91, no. 11, p. 4258–4272, 2006.

[21] B. Cronin, B. d. Wet and M. I. Wallace, "Lucky Imaging: Improved Localization Accuracy for Single Molecule Imaging," *Biophysical Journal,* vol. 96, p. 2912–2917, 2009.

[22] A. Yildiz, J. N. Forkey, S. A. McKinney, T. Ha, Y. E. Goldman and P. R. Selvin, "Myosin V Walks Hand-Over-Hand: Single Fluorophore Imaging with 1.5-nm Localization," *Science,* vol. 300, no. 5628, pp. 2061-2065, 2003.

[23] E. Betzig, G. H. Patterson, R. Sougrat, O. W. Lindwasser, S. Olenych, J. S. Bonifacino, M. W. Davidson, J. Lippincott-Schwartz and H. F. Hess, "Imaging Intracellular Fluorescent Proteins at Nanometer Resolution," *Science,* vol. 313, no. 5793, pp. 1642-1645, 2006.

[24] G. H. Patterson and J. Lippincott-Schwartz, "A photoactivatable GFP for selective photolabeling of proteins and cells," *Science,* vol. 297, no. 5588, pp. 1873-1877, 2002.

[25] M. Bates, B. Huang, G. T. Dempsey and X. Zhuang, "Multicolor super-resolution imaging with photo-switchable fluorescent probes," *Science,* vol. 317, no. 5845, pp. 1749-1753, 2007.

[26] B. Huang, W. Wang, M. Bates and X. Zhuang, "Three-dimension super-resolution imaging by stochastic optical reconstruction microscopy," *Science,* no. 319, pp. 810-813, 2008.

[27] W. Heisenberg, The Physical Principles of the Quantum Theory, Chicago University Press: Chicago, 1930.

[28] N. Bobroff, "Position measurement with a resolution and noise-limited instrument," vol. 6, no. 57, p. 1152–1157., 1986.

[29] "International vocabulary of metrology — Basic and general concepts and associated terms (VIM)," JCGM 200:2008.

[30] J. Engelhardt, J. Keller, P. Hoyer, M. Reuss and T. Staudt, "Molecular

Orientation Affects Localization Accuracy in Superresolution Far-Field Fluorescence Microscopy," *Nono Lett.*, vol. 11, no. 1, pp. 209-213, 2010.

[31] N. Brede, "Stochastic optical reconstruction microscopy(STORM): Characterization of factors that affect resolution, development of high speed analysis tools and application to intracellular transport," University of Heidelberg, 2011.

[32] A. H. Fischer, K. A. Jacobson, J. Rose and R. Zeller, "Preparation of Slides and Coverslips for Microscopy," in *Preparation of Cells and Tissues for Fluorescence Microscopy*, NY, USA, Cold Spring Harbor Laboratory Press, 2006, p. Chatper 4.

[33] "Lightning-Link Cy3 Antibody Labeling Products," [Online]. Available: http://www.novusbio.com/lightning-link-cy3-antibody-labeling.html.

[34] E. Matveeva, Z. Gryczynski and J. Malic, "Metal-enhanced fluorescence immunoassays using total internal reflection and silver island-coated surfaces," *Analytical Biochemistry*, no. 334, p. 303–311, 2004.

[35] H. Youk, A. Raj and A. v. Oudenaard, "Imaging Single mRNA Molecules in Yeast," *Methods in Enzymology*, vol. 470, pp. 429-446, 2010.

[36] "Accuracy and precision," Wikipedia, [Online]. Available: http://en.wikipedia.org/wiki/Accuracy_and_precision.

[37] "LENS DIFFRACTION & PHOTOGRAPHY," [Online]. Available: http://www.cambridgeincolour.com/tutorials/diffraction-photography.htm/.

[38] R. J. Ober, S. Ram and E. S. Ward, "Localization Accuracy in Single-Molecule Microscopy," *Biophysical Journal*, vol. 86, p. 1185–1200, 2004.

[39] J. S. Silfies , S. A. Schwartz and M. W. Davidson , "The Diffraction Barrier in Optical Microscopy," NIKON, [Online]. Available: http://www.microscopyu.com/articles/superresolution/diffractionbarrier.html.

[40] V. Westphal and S. W. Hell, "Nanoscale resolution in the focal plane of an optical microscope," *Physical review letters*, vol. 94, no. 143093, 2005.

[41] Y. Xu , "A Generic Smell Generating Enzymatic Biosensor," McMaster University, Hamilton, Ontario, 2011.

[42] J. Wichmann and S. W. Hell, "Breaking the diffraction resolution limit by stimulated emission: stimulated-emission-depletion fluorescence microscopy," *Optics Letters*, vol. 19, no. 11, pp. 780-782, 1994.

[43] "Introduction to Western Blotting," abdserotec, [Online]. Available: http://static.abdserotec.com/Lit-pdfs/Brochures1/westernblotbook.pdf.

[44] C. Moore, "Introduction to Western Blotting," AbD Serotec, [Online]. Available: http://static.abdserotec.com/Lit-pdfs/Brochures1/westernblotbook.pdf.

[45] McGraw-Hill Science & Technology Dictionary: orientation polarization.

[46] "Orientation and Rotational Motions of Single Molecules by Polarized Total Internal Reflection Fluorescence Microscopy (polTIRFM)," [Online]. Available: http://cshprotocols.cshlp.org/content/2012/5/pdb.top069344.full.

[47] "Orientation Polarization," [Online]. Available: http://www.tf.uni-kiel.de/matwis/amat/elmat_en/kap_3/backbone/r3_2_4.html.

[48] "Super resolution techniques," [Online]. Available: http://online.physics.uiuc.edu/courses/phys598om/spring12/Lectures/files/Lecture%2026%20Super%20resolution%20Structured%20Illumination%20Storm%20etc/STEDDiscussion.pdf.